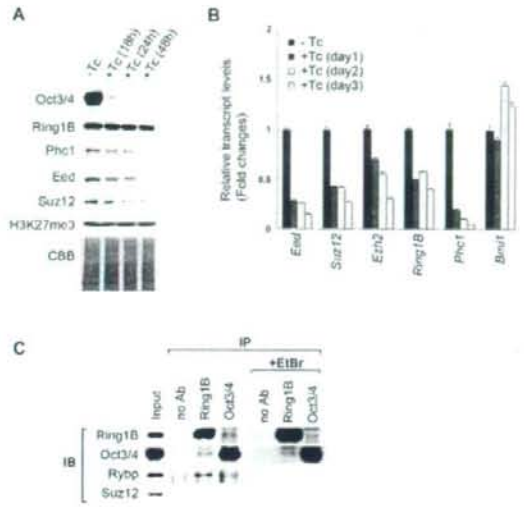

Fig. 5. Possible mechanisms for the reduction in Ring1B binding upon Oct3/4 depletion or differentiation cues. (**A**) Western blot demonstrating changes in the levels of Oct3/4, Ring1B, Phc1, Eed, Suz12 and H3K27me3 after conditional deletion of *Oct3/4* by tetracycline (Tc) treatment of ZHBTc4 ES cells. (**B**) Changes in gene expression levels for *Eed*, *Suz12*, *Ezh2*, *Ring1B*, *Phc1* and *Bmi1* after tetracycline treatment (+Tc) of ZHBTc4 ES cells were determined by real-time PCR, normalized to an *Actb* control and depicted as fold changes relative to the tetracycline-untreated (–Tc) ES cells. Error bars are based on the s.d. derived from triplicate PCR reactions. (**C**) Physical interaction of Ring1B and Oct3/4 in wild-type ES cells demonstrated by reciprocal immunoprecipitation/immunoblot analyses. Antibodies used for immunoprecipitation (IP, top) and immunoblotting (IB, side) are indicated. The association between Ring1B and Oct3/4 proteins remains intact in the presence of ethidium bromide (+EtBr), a DNA-intercalating drug that can disassociate proteins from DNA.

transcription, apoptosis and cell cycle (Fig. 6B). Therefore, a subset of genes induced by enforced Gata6 activation is correlated with those regulated by Oct3/4 and Ring1A/B, suggesting an extension of the functional link to Gata6.

We then investigated whether Gata6 activation affects the levels of Ring1B and Eed at selected Polycomb targets. Of the selected genes, the expression level was increased for *Gata6*, *Cdx2*, *Zic1* and *T*, whereas it was reduced or unchanged for *Hoxb8* and *Hand1* upon Gata6 expression (data not shown). Ring1B binding was significantly reduced irrespective of transcriptional status (Fig. 6C). Phc1 and Eed binding was also reduced (Fig. 6C), consistent with the observed reduction in protein levels (Fig. 6A). These results indicate that Gata6 activation impacts upon gene expression in similar manner to Oct3/4 depletion. Therefore, it is likely that the local engagement of PRC1 depends on the core transcriptional regulatory circuitry rather than solely on Oct3/4 in ES cells.

DISCUSSION

In this study, we first demonstrate that Ring1A/B are required to maintain ES cells in an undifferentiated state by repressing the expression of developmental regulators that direct differentiation of ES cells. This process involves local inhibition of chromatin remodeling via direct binding of PRC1. We further show that Ring1A/B-mediated PcG silencing is hierarchically linked to the core transcriptional regulatory circuitry and that this linkage can be abolished by developmental cues that negatively regulate the core circuitry (Fig. 7). Developmental regulators repressed by this epistatic link, such as *Cdx2* and *Gata6*, are shown to be predisposed for active transcription. Active and reversible repression by this epistatic link is important to potentiate ES cells so that they can respond to developmental cues appropriately and, consequently, it may underpin the maintenance of pluripotency. Therefore, our data show that Ring1A/B are instrumental for the core transcriptional regulatory circuitry to maintain ES cell identity.

The dissociation of PRC1 as a prerequisite for subsequent association of chromatin remodeling components

These and previous studies suggest that PcG proteins are linked to the core transcriptional regulatory circuitry at multiple levels (Fig. 3) (Lee et al., 2006). Oct3/4 is likely to recruit Ring1B to its targets via direct interactions and also to induce the expression of PRC1 components via a transcriptional regulatory mechanism (Fig. 5). Moreover, it is notable that Oct3/4 loss displaces Ring1B from most of its target genes, which are not necessarily functional targets of Oct3/4 (Fig. 4C). This prompts us to postulate an activity that modulates Ring1B recruitment under the regulation of Oct3/4. Indeed, the RING1 and YY1 binding protein, Rybp, potentially fulfils such a linking role between Oct3/4 and Ring1B because Rybp is able to form complexes with both proteins (Fig. 5C) (Wang et al., 2006). Such multiple interactions might enable coordinated displacement of PRC1 and PRC2 from their target genes upon disruption of the core circuitry by differentiation cues. Since forced depletion of *Ring1A/B* leads to spontaneous differentiation of ES cells, dissociation of PRC1 from the targets may be functionally implicated in the differentiation process. We presume that the dissociation of PRC1 and PRC2 is a prerequisite for the subsequent association of other chromatin modifiers such as Trithorax group proteins, which catalyze local hypertrimethylation of H3K4 upon Oct3/4 depletion (Dou et al., 2005; Wysocka et al., 2003). This is supported by our results shown in Fig. 2C, and by previous experiments showing that the SWI-SNF complex is unable to remodel polynucleosomal templates bound by PRC1 in vitro (Shao et al., 1999). Therefore, the global enhancement of chromatin remodeling at developmental genes might be one of the essential events in promoting proper differentiation of ES cells.

Implications from the reversibility of Polycomb binding in the balance of self-renewal versus differentiation

The reversibility of Polycomb binding to the targets regulated by the core transcriptional regulatory circuitry and by differentiation cues might confer self-renewing and differentiation capacities to ES cells. Intriguingly, PcG silencing has been suggested to be involved in the function and maintenance of tissue stem and cancer cells, which are also characterized by both self-renewal and differentiation potency (Lessard and Sauvageau, 2003; Molofsky et al., 2003; Ohta et al., 2002; Park et al., 2003; Villa et al., 2007). For example, *Bmi1* loss promotes differentiation of hematopoietic stem cells (HSCs) and premature senescence of neural stem cells, whereas forced expression of *Bmi1* enhances symmetrical cell division of HSCs (Iwama et al., 2004; Molofsky et al., 2005).

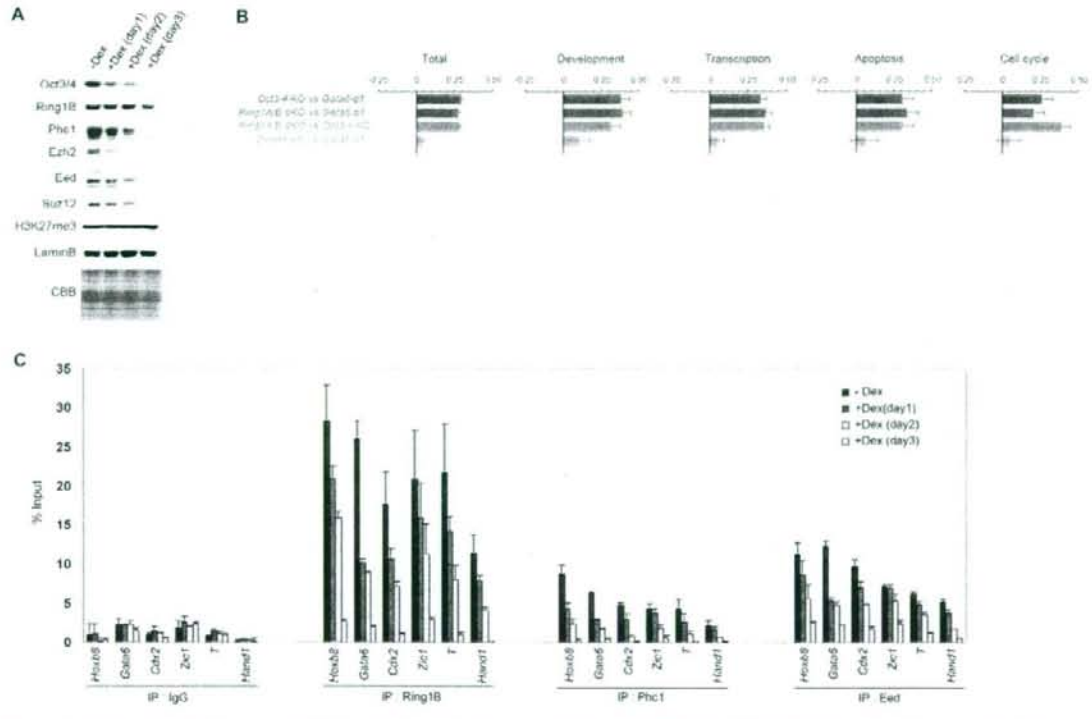

Fig. 6. The engagement of PRC1 and PRC2 is gradually decreased upon Gata6-mediated differentiation of ES cells into primitive endoderm lineages. (**A**) Western blot analysis demonstrating changes in the levels of Oct3/4, Ring1B, Phc1, Ezh2, Eed, Suz12 and H3K27me3 after conditional activation of Gata6 by dexamethasone (Dex) treatment of G6GR ES cells. Lamin B and CBB staining confirmed equal loading. (**B**) Significant overlap of expression profiles in *Ring1A/B*-dKO (day 4), *Oct3/4*-KO (day 1) and Gata6-differentiated (day 2) ES cells. Pearson's correlation of expression changes for probes that belong to specific GO classifications are shown by bars. Functional groupings are indicated above each graph. Error bars represent 95% confidence intervals of correlation coefficients calculated by Z transformation. (**C**) ChIP analysis showing binding of Ring1B, Phc1 and Eed at the promoter regions of the selected target genes after Dex treatment in G6GR ES cells. The relative amount of immunoprecipitated DNA is depicted as a percentage of input. Error bars represent s.d. determined from at least three independent experiments.

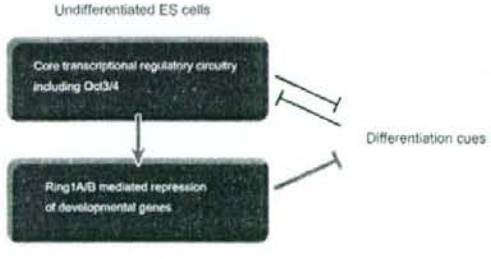

Fig. 7. Schematic representation of the interaction between Ring1A/B and the core transcriptional regulatory circuitry in mouse ES cells. Ring1A/B-mediated PcG silencing functions downstream of the core transcriptional regulatory circuitry including Oct3/4. Developmental cues, such as *Gata6* activation, downregulate the activity of the core transcriptional regulatory circuitry, which accompanies a global decrease in PcG silencing.

Recently, it has been reported that knockdown of *SUZ12* in acute promyelocytic leukemic cells results in myeloid differentiation (Villa et al., 2007). It is thus likely that similar molecular mechanisms identified in ES cells that involve *Ring1A/B* might operate in the maintenance and differentiation of various tissue stem cells and cancer cells. Since *Oct3/4* and *Nanog* are not expressed in most somatic cells, other downstream effectors expressed in common among the stem cells might be more directly involved in the regulation of Polycomb binding. Alternatively, other factors specifically expressed in tissue and/or cancer stem cells might substitute for the action of *Oct3/4* or *Nanog*. Further studies will be needed to clarify these issues.

We thank Hitoshi Niwa for providing ZHBTc4, G6GR and ZHTc6 cells. This work was supported in part by a grant from the Genome Network Project (to H.K.) and a grant-in-aid for Scientific Research on Priority Areas (17045038, to M.E.) from the Ministry of Education, Culture, Sports, Science and Technology, Japan.

Supplementary material

Supplementary material for this article is available at http://dev.biologists.org/cgi/content/full/135/8/1513/DC1

References

Androutsellis-Theotokis, A., Leker, R. R., Soldner, F., Hoeppner, D. J., Ravin, R., Poser, S. W., Rueger, M. A., Bae, S. K., Kittappa, R. and McKay, R. D. (2006). Notch signalling regulates stem cell numbers in vitro and in vivo. *Nature* **442**, 823-826.

Atsuta, T., Fujimura, S., Moriya, H., Vidal, M., Akasaka, T. and Koseki, H. (2001). Production of monoclonal antibodies against mammalian Ring1B proteins. *Hybridoma* **20**, 43-46.

Auernhammer, C. J. and Melmed, S. (2000). Leukemia-inhibitory factor-neuroimmune modulator of endocrine function. *Endocr. Rev.* **21**, 313-345.

Avilion, A. A., Nicolis, S. K., Pevny, L. H., Perez, L., Vivian, N. and Lovell-Badge, R. (2003). Multipotent cell lineages in early mouse development depend on SOX2 function. *Genes Dev.* **17**, 126-140.

Azuara, V., Perry, P., Sauer, S., Spivakov, M., Jorgensen, H. F., John, R. M., Gouti, M., Casanova, M., Warnes, G., Merkenschlager, M. et al. (2006). Chromatin signatures of pluripotent cell lines. *Nat. Cell Biol.* **8**, 532-538.

Bernstein, B. E., Mikkelsen, T. S., Xie, X., Kamal, M., Huebert, D. J., Cuff, J., Fry, B., Meissner, A., Wernig, M., Plath, K. et al. (2006). A bivalent chromatin structure marks key developmental genes in embryonic stem cells. *Cell* **125**, 315-326.

Bolstad, B. M., Irizarry, R. A., Astrand, M. and Speed, T. P. (2003). A comparison of normalization methods for high density oligonucleotide array data based on variance and bias. *Bioinformatics* **19**, 185-193.

Boyer, L. A., Lee, T. I., Cole, M. F., Johnstone, S. E., Levine, S. S., Zucker, J. P., Guenther, M. G., Kumar, R. M., Murray, H. L., Jenner, R. G. et al. (2005). Core transcriptional regulatory circuitry in human embryonic stem cells. *Cell* **122**, 947-956.

Boyer, L. A., Plath, K., Zeitlinger, J., Brambrink, T., Medeiros, L. A., Lee, T. I., Levine, S. S., Wernig, M., Tajonar, A., Ray, M. K. et al. (2006). Polycomb complexes repress developmental regulators in murine embryonic stem cells. *Nature* **441**, 349-353.

Buchwald, G., van der Stoop, P., Weichenrieder, O., Perrakis, A., van Lohuizen, M. and Sixma, T. K. (2006). Structure and E3-ligase activity of the Ring-Ring complex of polycomb proteins Bmi1 and Ring1b. *EMBO J.* **25**, 2465-2474.

Burdon, T., Smith, A. and Savatier, P. (2002). Signalling, cell cycle and pluripotency in embryonic stem cells. *Trends Cell Biol.* **12**, 432-438.

Cales, C., Roman-Trufero, M., Pavon, L., Serrano, I., Melgar, T., Endoh, M., Perez, C., Koseki, H. and Vidal, M. (2008). Inactivation of the polycomb group protein Ring1B unveils an antiproliferative role in hematopoietic cell expansion and cooperation with tumorigenesis associated with Ink4a deletion. *Mol. Cell. Biol.* **28**, 1018-1028.

Cao, R., Wang, L., Wang, H., Xia, L., Erdjument-Bromage, H., Tempst, P., Jones, R. S. and Zhang, Y. (2002). Role of histone H3 lysine 27 methylation in Polycomb-group silencing. *Science* **298**, 1039-1043.

Catena, R., Tiveron, C., Ronchi, A., Porta, S., Ferri, A., Tatangelo, L., Cavallaro, M., Favaro, R., Ottolenghi, S., Reinbold, R. et al. (2004). Conserved POU binding DNA sites in the Sox2 upstream enhancer regulate gene expression in embryonic and neural stem cells. *J. Biol. Chem.* **279**, 41846-41857.

Chambers, I., Colby, D., Robertson, M., Nichols, J., Lee, S., Tweedie, S. and Smith, A. (2003). Functional expression cloning of Nanog, a pluripotency sustaining factor in embryonic stem cells. *Cell* **113**, 643-655.

Chazaud, C., Yamanaka, Y., Pawson, T. and Rossant, J. (2006). Early lineage segregation between epiblast and primitive endoderm in mouse blastocysts through the Grb2-MAPK pathway. *Dev. Cell* **10**, 615-624.

Czermin, B., Melfi, R., McCabe, D., Seitz, V., Imhof, A. and Pirrotta, V. (2002). Drosophila enhancer of Zeste/ESC complexes have a histone H3 methyltransferase activity that marks chromosomal Polycomb sites. *Cell* **111**, 185-196.

Dou, Y., Milne, T. A., Tackett, A. J., Smith, E. R., Fukuda, A., Wysocka, J., Allis, C. D., Chait, B. T., Hess, J. L. and Roeder, R. G. (2005). Physical association and coordinate function of the H3 K4 methyltransferase MLL1 and the H4 K16 acetyltransferase MOF. *Cell* **121**, 873-885.

de Napoles, M., Mermoud, J. E., Wakao, R., Tang, Y. A., Endoh, M., Appanah, R., Nesterova, T. B., Silva, J., Otte, A. P., Vidal, M. et al. (2004). Polycomb group proteins Ring1A/B link ubiquitylation of histone H2A to heritable gene silencing and X inactivation. *Dev. Cell* **7**, 663-676.

del Mar Lorente, M., Marcos-Gutierrez, C., Perez, C., Schoorlemmer, J., Ramirez, A., Magin, T. and Vidal, M. (2000). Loss- and gain-of-function mutations show a polycomb group function for Ring1A in mice. *Development* **127**, 5093-5100.

Evans, M. J. and Kaufman, M. H. (1981). Establishment in culture of pluripotential cells from mouse embryos. *Nature* **292**, 154-156.

Fischle, W., Wang, Y., Jacobs, S. A., Kim, Y., Allis, C. D. and Khorasanizadeh, S. (2003). Molecular basis for the discrimination of repressive methyl-lysine marks in histone H3 by Polycomb and HP1 chromodomains. *Genes Dev.* **17**, 1870-1881.

Fujikura, J., Yamato, E., Yonemura, S., Hosoda, K., Masui, S., Nakao, K., Miyazaki, J.-i., and Niwa, H. (2002). Differentiation of embryonic stem cells is induced by GATA factors. *Genes Dev.* **16**, 784-789.

Fujimura, Y., Isono, K., Vidal, M., Endoh, M., Kajita, H., Mizutani-Koseki, Y., Takihara, Y., van Lohuizen, M., Otte, A., Jenuwein, T. et al. (2006). Distinct roles of Polycomb group gene products in transcriptionally repressed and active domains of Hoxb8. *Development* **133**, 2371-2381.

Garcia, E., Marcos-Gutierrez, C., del Mar Lorente, M., Moreno, J. C. and Vidal, M. (1999). RYBP, a new repressor protein that interacts with components of the mammalian Polycomb complex, and with the transcription factor YY1. *EMBO J.* **18**, 3404-3418.

Hamer, K. M., Sewalt, R. G., den Blaauwen, J. L., Hendrix, T., Satijn, D. P. and Otte, A. P. (2002). A panel of monoclonal antibodies against human polycomb group proteins. *Hybrid Hybridomics* **21**, 245-252.

Heinrich, P. C., Behrmann, I., Haan, S., Hermanns, H. M., Muller-Newen, G. and Schaper, F. (2003). Principles of interleukin (IL)-6-type cytokine signalling and its regulation. *Biochem. J.* **374**, 1-20.

Isono, K., Fujimura, Y.-i, Shinga, J., Yamaki, M., O-Wang, J., Takihara, Y., Murahashi, Y., Takada, Y., Mizutani-Koseki, Y. and Koseki, H. (2005a). Mammalian polyhomeotic homologues Phc2 and Phc1 act in synergy to mediate polycomb repression of Hox genes. *Mol. Cell. Biol.* **25**, 6694-6706.

Isono, K., Mizutani-Koseki, Y., Komori, T., Schmidt-Zachmann, M. S. and Koseki, H. (2005b). Mammalian polycomb-mediated repression of Hox genes requires the essential spliceosomal protein Sf3b1. *Genes Dev.* **19**, 536-541.

Iwama, A., Oguro, H., Negishi, M., Kato, Y., Morita, Y., Tsukui, H., Ema, H., Kamijo, T., Katoh-Fukui, Y., Koseki, H. et al. (2004). Enhanced self-renewal of hematopoietic stem cells mediated by the polycomb gene product Bmi-1. *Immunity* **21**, 843-851.

Kuroda, T., Tada, M., Kubota, H., Kimura, H., Hatano, S. Y., Suemori, H., Nakatsuji, N. and Tada, T. (2005). Octamer and Sox elements are required for transcriptional cis regulation of Nanog gene expression. *Mol. Cell. Biol.* **25**, 2475-2485.

Kuzmichev, A., Nishioka, K., Erdjument-Bromage, H., Tempst, P. and Reinberg, D. (2002). Histone methyltransferase activity associated with a human multiprotein complex containing the Enhancer of Zeste protein. *Genes Dev.* **16**, 2893-2905.

Lai, J. S. and Herr, W. (1992). Ethidium bromide provides a simple tool for identifying genuine DNA-independent protein associations. *Proc. Natl. Acad. Sci. USA* **89**, 6958-6962.

Lee, T. I., Jenner, R. G., Boyer, L. A., Guenther, M. G., Levine, S. S., Kumar, R. M., Chevalier, B., Johnstone, S. E., Cole, M. F., Isono, K. et al. (2006). Control of developmental regulators by Polycomb in human embryonic stem cells. *Cell* **125**, 301-313.

Leeb, M. and Wutz, A. (2007). Ring1B is crucial for the regulation of developmental control genes and PRC1 proteins but not X inactivation in embryonic cells. *J. Cell Biol.* **178**, 219-229.

Lei, H., Oh, S. P., Okano, M., Juttermann, R., Goss, K. A., Jaenisch, R. and Li, E. (1996). De novo DNA cytosine methyltransferase activities in mouse embryonic stem cells. *Development* **122**, 3195-3205.

Lessard, J. and Sauvageau, G. (2003). Bmi-1 determines the proliferative capacity of normal and leukaemic stem cells. *Nature* **423**, 255-260.

Loh, Y. H., Wu, Q., Chew, J. L., Vega, V. B., Zhang, W., Chen, X., Bourque, G., George, J., Leong, B., Liu, J. et al. (2006). The Oct4 and Nanog transcription network regulates pluripotency in mouse embryonic stem cells. *Nat. Genet.* **38**, 431-440.

Martin, G. R. (1981). Isolation of a pluripotent cell line from early mouse embryos cultured in medium conditioned by teratocarcinoma stem cells. *Proc. Natl. Acad. Sci. USA* **78**, 7634-7638.

Matoba, R., Niwa, H., Masui, S., Ohtsuka, S., Carter, M. G., Sharov, A. A. and Ko, M. S. (2006). Dissecting oct3/4-regulated gene networks in embryonic stem cells by expression profiling. *PLoS ONE* **1**, e26.

Min, J., Zhang, Y. and Xu, R. M. (2003). Structural basis for specific binding of Polycomb chromodomain to histone H3 methylated at Lys 27. *Genes Dev.* **17**, 1823-1828.

Mitsui, K., Tokuzawa, Y., Itoh, H., Segawa, K., Murakami, M., Takahashi, K., Maruyama, M., Maeda, M. and Yamanaka, S. (2003). The homeoprotein Nanog is required for maintenance of pluripotency in mouse epiblast and ES cells. *Cell* **113**, 631-642.

Miyagishima, H., Isono, K., Fujimura, Y., Iyo, M., Takihara, Y., Masumoto, H., Vidal, M. and Koseki, H. (2003). Dissociation of mammalian Polycomb-group proteins, Ring1B and Rae28/Ph1, from the chromatin correlates with configuration changes of the chromatin in mitotic and meiotic prophase. *Histochem. Cell Biol.* **120**, 111-119.

Molofsky, A. V., Pardal, R., Iwashita, T., Park, I. K., Clarke, M. F. and Morrison, S. J. (2003). Bmi-1 dependence distinguishes neural stem cell self-renewal from progenitor proliferation. *Nature* **425**, 962-967.

Molofsky, A. V., He, S., Bydon, M., Morrison, S. J. and Pardal, R. (2005). Bmi-1 promotes neural stem cell self-renewal and neural development but not mouse growth and survival by repressing the p16Ink4a and p19Arf senescence pathways. *Genes Dev.* **19**, 1432-1437.

Muller, J., Hart, C. M., Francis, N. J., Vargas, M. L., Sengupta, A., Wild, B., Miller, E. L., O'Connor, M. B., Kingston, R. E. and Simon, J. A. (2002).

Histone methyltransferase activity of a Drosophila Polycomb group repressor complex. *Cell* **111**, 197-208.

Nichols, J., Zevnik, B., Anastassiadis, K., Niwa, H., Klewe-Nebenius, D., Chambers, I., Scholer, H. and Smith, A. (1998). Formation of pluripotent stem cells in the mammalian embryo depends on the POU transcription factor Oct4. *Cell* **95**, 379-391.

Niwa, H., Miyazaki, J. and Smith, A. G. (2000). Quantitative expression of Oct-3/4 defines differentiation, dedifferentiation or self-renewal of ES cells. *Nat. Genet.* **24**, 372-376.

Niwa, H., Toyooka, Y., Shimosato, D., Strumpf, D., Takahashi, K., Yagi, R. and Rossant, J. (2005). Interaction between Oct3/4 and Cdx2 determines trophectoderm differentiation. *Cell* **123**, 917-929.

Ohta, H., Sawada, A., Kim, J. Y., Tokimasa, S., Nishiguchi, S., Humphries, R. K., Hara, J. and Takihara, Y. (2002). Polycomb group gene rae28 is required for sustaining activity of hematopoietic stem cells. *J. Exp. Med.* **195**, 759-770.

Okumura-Nakanishi, S., Saito, M., Niwa, H. and Ishikawa, F. (2005). Oct-3/4 and Sox2 regulate Oct-3/4 gene in embryonic stem cells. *J. Biol. Chem.* **280**, 5307-5317.

Orlando, V., Strutt, H. and Paro, R. (1997). Analysis of chromatin structure by in vivo formaldehyde cross-linking. *Methods* **11**, 205-214.

Park, I. K., Qian, D., Kiel, M., Becker, M. W., Pihalja, M., Weissman, I. L., Morrison, S. J. and Clarke, M. F. (2003). Bmi-1 is required for maintenance of adult self-renewing haematopoietic stem cells. *Nature* **423**, 302-305.

Rodda, D. J., Chew, J. L., Lim, L. H., Loh, Y. H., Wang, B., Ng, H. H. and Robson, P. (2005). Transcriptional regulation of nanog by OCT4 and SOX2. *J. Biol. Chem.* **280**, 24731-24737.

Seibler, J., Zevnik, B., Kuter-Luks, B., Andreas, S., Kern, H., Hennek, T., Rode, A., Heimann, C., Faust, N., Kauselmann, G. et al. (2003). Rapid generation of inducible mouse mutants. *Nucleic Acids Res.* **31**, e12.

Shao, Z., Raible, F., Mollaaghababa, R., Guyon, J. R., Wu, C. T., Bender, W. and Kingston, R. E. (1999). Stabilization of chromatin structure by PRC1, a Polycomb complex. *Cell* **98**, 37-46.

Shimosato, D., Shiki, M. and Niwa, H. (2007). Extra-embryonic endoderm cells derived from ES cells induced by GATA Factors acquire the character of XEN cells. *BMC Dev Biol.* **7**, 80.

Villa, R., Pasini, D., Gutierrez, A., Morey, L., Occhionorelli, M., Vire, E., Nomdedeu, J. F., Jenuwein, T., Pelicci, P. G., Minucci, S. et al. (2007). Role of the polycomb repressive complex 2 in acute promyelocytic leukemia. *Cancer Cell* **11**, 513-525.

Wang, H., Wang, L., Erdjument-Bromage, H., Vidal, M., Tempst, P., Jones, R. S. and Zhang, Y. (2004). Role of histone H2A ubiquitination in Polycomb silencing. *Nature* **431**, 873-878.

Wang, J., Rao, S., Chu, J., Shen, X., Levasseur, D. N., Theunissen, T. W. and Orkin, S. H. (2006). A protein interaction network for pluripotency of embryonic stem cells. *Nature* **444**, 364-368.

Williams, R. L., Hilton, D. J., Pease, S., Willson, T. A., Stewart, C. L., Gearing, D. P., Wagner, E. F., Metcalf, D., Nicola, N. A. and Gough, N. M. (1988). Myeloid leukaemia inhibitory factor maintains the developmental potential of embryonic stem cells. *Nature* **336**, 684-687.

Wysocka, J., Myers, M. P., Laherty, C. D., Eisenman, R. N. and Herr, W. (2003). Human Sin3 deacetylase and trithorax-related Set1/Ash2 histone H3-K4 methyltransferase are tethered together selectively by the cell-proliferation factor HCF-1. *Genes Dev.* **17**, 896-911.

Published online 1 April 2008

Nucleic Acids Research, 2008, Vol. 36, No. 9 **2939–2947**
doi:10.1093/nar/gkn146

A polycomb group protein, PHF1, is involved in the response to DNA double-strand breaks in human cell

Zehui Hong[1], Jie Jiang[1], Li Lan[1], Satoshi Nakajima[1], Shin-ichiro Kanno[1], Haruhiko Koseki[2] and Akira Yasui[1,*]

[1]Department of Molecular Genetics, Institute of Development, Aging and Cancer, Tohoku University, Seiryomachi 4-1, Aobaku, Sendai 980-8575 and [2]Laboratory of Developmental Genetics, Riken Research Center for Allergy and Immunology, Suehiro-cho 1-7-22, Tsurumi-ku, Yokohama 230-0045, Japan

Received December 18, 2007; Revised March 4, 2008; Accepted March 17, 2008

ABSTRACT

DNA double-strand breaks (DSBs) represent the most toxic DNA damage arisen from endogenous and exogenous genotoxic stresses and are known to be repaired by either homologous recombination or nonhomologous end-joining processes. Although many proteins have been identified to participate in either of the processes, the whole processes still remain elusive. Polycomb group (PcG) proteins are epigenetic chromatin modifiers involved in gene silencing, cancer development and the maintenance of embryonic and adult stem cells. By screening proteins responding to DNA damage using laser micro-irradiation, we found that PHF1, a human homolog of *Drosophila* polycomb-like, Pcl, protein, was recruited to DSBs immediately after irradiation and dissociated within 10 min. The accumulation at DSBs is Ku70/Ku80-dependent, and knockdown of PHF1 leads to X-ray sensitivity and increases the frequency of homologous recombination in HeLa cell. We found that PHF1 interacts physically with Ku70/Ku80, suggesting that PHF1 promotes non-homologous end-joining processes. Furthermore, we found that PHF1 interacts with a number of proteins involved in DNA damage responses, RAD50, SMC1, DHX9 and p53, further suggesting that PHF1, besides the function in PcG, is involved in genome maintenance processes.

INTRODUCTION

DNA double-strand breaks (DSBs) can be caused by both cell-intrinsic sources, such as replication errors or reactive oxygen species, and a variety of extrinsic factors, including ionizing radiation (IR) and radiomimetic chemicals. DSBs representing the most toxic DNA lesions, if left unrepaired, may cause cell death and genomic instability. Inefficient or inaccurate repair may lead to mutation and/or chromosome rearrangement, and predisposition to cancer (1–5). DSBs also represent obligatory intermediates of physiological DNA rearrangement processes taking place during the development and maturation of the adaptive immune system, V(D)J recombination and immunoglobulin (Ig) heavy-chain class switch recombination (CSR) (6). Therefore, defects in the repair of these DNA breaks can cause profound immuno-deficiencies (7).

Eukaryotes cells have evolved two major pathways for repairing DSBs, homologous recombination (HR) and nonhomologous end joining (NHEJ). Both pathways are conserved from yeast to mammals and function in complementary ways to repair DSBs (1,5,8). During HR, DSBs are repaired through a precise pathway that uses homologous sequence usually provided by the sister chromatid during replication as for template. In contrast, NHEJ is an error-prone repair pathway that joins ends together without the requirement for significant sequence homology (1,5,8). Once DSBs are produced, cells trigger a series of signaling pathway including cycle regulation, transcription, histone modification and apoptosis that have direct or indirect effect on DSB repair. Following DNA damage, the DNA damage sensors ATM/ATR and DNA-PK phosphorylate CHK1 and CHK2 to regulate cell cycle checkpoint, phosphorylate P53 to activate apoptosis signal pathway, phosphorylate H2AX and a number of proteins involved in DSB repair such as NBS1 and SMC1 (5,9). Besides phosphorylation of H2AX, recently, histone ubiquitinations, acetylations and methylations have been implicated in the DNA damage checkpoint and DSBs repair pathways (10). Although the last few years a wealth of new information has been produced about DSBs damage response and DNA repair, and many novel proteins involved in the process have been identified, the process still remains elusive.

*To whom correspondence should be addressed. Tel: +81 22 717 8465; Fax: +81 22 717 8470; Email: ayasui@idac.tohoku.ac.jp

With the aim of identifying new factors involved in DSBs damage response and repair of mammalian cells, we screened a number of proteins involved in chromatin remodeling and regulation by using laser micro-irradiation system (11–13). PcG proteins are epigenetic chromatin modifiers involved in transcription regulation, maintenance of embryonic and adult stem cells and cancer development (14,15). PcG genes were first identified by their requirement for the maintenance of the stable repression of Hox genes during the development of *Drosophila melanogaster* and are highly conserved throughout evolution. In mammals, PcG genes are also implicated in Homeobox (Hox) gene regulation. Their biological activity lies in stable silencing of specific sets of genes through chromatin modifications. Recently, emerging evidence implicates the PcG proteins in cellular proliferation and tumorigenesis (15–18). Furthermore, overexpression of a PcG protein, EZH2, in breast epithelial cells reduced Rad51 paralogs both in the mRNA and protein levels which are required for proper HR DNA repair (19), and heterozygosity for mutations in either extra sex combs (Esc) or Enhance of Polycomb [E(PC)] increases the lever of HR and enhances genome stability in somatic cells of *D. melanogaster* (20).

Laser micro-irradiation makes it possible to introduce various types of DNA damage at restricted regions in the nucleus of a single cell and to analyze the response of proteins to the damage with antibody by immuno-staining or with transfected GFP-tagged proteins under microscope in a real-time image. So far as laser light dose and exposed time are extremely limited, there is no effect of heat production. The major product of irradiation with UVA laser light is DNA damage, because UVA laser light is either absorbed directly by DNA or by photosensitizers around DNA creating radicals, which attack DNA. Therefore, major types of DNA damage produced by UVA laser irradiation are oxidative ones, and with increasing laser dose and by addition of photosensitizers, DNA single-strand breaks, DSBs and base damage can be produced effectively (11,12,21).

For the reason that both PcG proteins play important roles in tumorigenesis, and some of PcG proteins are shown by genetic analysis to be involved in DSBs damage response, we analyzed whether or not PcG proteins are directly involved in the response to DSBs. We found that PHD finger Protein 1 (PHF1) is recruited rapidly to DSBs sites, that is dependent on Ku70/Ku80, and demonstrated that PHF1 is associated with Ku70/Ku80, Rad50, DHX9, SMC1 and P53 besides PcG proteins. Furthermore, knockdown of PHF1 leads to X-ray sensitivity and increases HR frequency. These data suggest that PHF1 is involved in DSBs damage response and may play an important role in NHEJ and maintaining genome stability.

MATERIALS AND METHODS

Construction of plasmids for expression of various genes

Plasmids expressing human genes encoding KU70, KU80, XRCC4, LigaseIV, Artemis, XLF, RAD52 and NBS1 were constructed by cloning cDNA amplified from HeLa cells. PHF1 (isoform 2) was amplified from a human cDNA clone (no. MGC: BC008834). We modified the multiple cloning sites of vectors EGFP-C1, EGFP-N1 to introduce various cDNAs attached with an in-frame XhoI or SalI site at the start and NotI site at the stop codons. Deletion fragments of PHF1 were generated by PCR amplification, and then cloned into vectors. All constructs were verified by sequencing.

Cell lines, culture and transfection

The following cell lines were used in this study: HeLa; V79B; XR-V15B (Ku80$^{-/-}$ CHO cell line); CHO9; XR-C1 (DNA-PKcs$^{-/-}$ CHO cell line); XR-1 (XRCC4$^{-/-}$ CHO cell line); 1022QVAP81 (NBS1-deficient human cell line); Flp-In-293 (Invitrogen), All cell lines were propagated in Dulbecco's modified-MEM (Nissui), supplemented with 1 mM L-glutamine and 10% fetal bovine serum at 37°C and 5% CO_2. For suspension culture, cells were grown in Joklik medium (Sigma) supplemented with 5% fetal bovine serum at 37°C in spinner flask. Caps of spinner flask should be tightly closed and density of cells was kept between 2 and -6×10^5/ml. For UVA-laser irradiation, cells were plated in glass-bottomed dishes (Matsunami Glass) and transfected with expression vectors using fuGene6 (Roche), according to the manufacturer's protocol.

Microscopy and UVA-laser irradiation

Fluorescence images were obtained and processed using a confocal scanning laser microscopy system (FV-500, Olympus). UVA-laser irradiation was used to induce DSBs in cultured cells as described previously (11–13). Briefly, cells in glass-bottomed dishes were micro-irradiated with a 405 nm pulse laser (Olympus) along a user-defined path. Laser was focused through a 40× objective lens and the treatment dose was controlled by number of scans used. A single laser scan at full power delivers about 1600 nW. Cells were treated with 10 nM 5-bromo-2-deoxyuridine (BrdU) during 24 h prior to irradiation. Given the low treatment doses and the wavelength used, the influence of the laser light on DNA is mainly indirect via photosensitization of natural or added (BrdU) chromophores near the DNA within cell. The irradiation dose was fixed in the experiments as 500 scans in the presence of BrdU, which produces more than 10^3 DSBs per cell, which corresponds to 30 Gy of X-ray irradiation to a human cell. The number of DSBs was determined by comparison of the number of γH2AX produced by laser micro-irradiation with that produced by X-Ray irradiation, based on the method reported before (48).

Immunofluorescence

Cells were fixed in cold methanol/acetone (1:1) for 10 min at −20°C and probed with mouse anti-PHF1 (1:30; M01, Abnova), mouse anti-γH2AX (1:400; jbw103, Upstate). The secondary antibody used was Alexa fluor 594 anti-mouse IgG (1:400; molecular Probes). Nuclear DNA was stained with 4′,6′-diamidino-2-phenylindole (DAPI; 0.5 μg/ml, Wako). Fluorescence microscopy was

performed using the same microscopy as used in laser micro-irradiation.

Immunoblotting

Cells were sonicated in lysis buffer (50 mM Tris–HCl, pH 7.5, 0.15 M NaCl, 0.5% NP-40, 1 mM EDTA) supplemented with protease inhibitor (complete, EDTA-free, Roche) and cleared by centrifugation. Proteins were separated by SDS/PAGE, electroblotted and detected with the following antibodies: mouse anti-PHF1 (1:1000; M01, Abnova), mouse anti-Ku70 (1:3000; N3H10, Sigma), mouse anti-FLAG (1:3000; F-3165, Sigma), goat anti-actin (1:2000; I-19, Santa Cruz Biotechnology), mouse anti-P53 (1:1000; DO-1, Santa Cruz Biotechnology), rabbit anti-RbAP46 (1:1000; PA1-868, ABR) and rabbit anti-SMC1 (1:1000; BL308, Bethyl). The secondary antibodies used were from Santa Cruz Biotechnology: anti-rabbit IgG-HRP (1:3000, sc-2004), anti-mouse IgG-HRP (1:3000, sc-2005) and anti-goat IgG-HRP (1:3000, sc-2056).

Stable cell lines

Stable isogenic cell lines expressing either PHF1 or Ku80 tagged with a FLAG-HA were established using Flp-In system (Invitrogen), according to the manufacturer's protocol. Briefly, we modified pcDNA5/FRT vector (Invitrogen) to introduce various cDNAs attached with an in-frame XhoI site at the start and NotI site at the stop codons and put two different epitope tags in tandem (FLAG-HA) on the 5′-terminus of cloning site. Flp-In-293 cells were cotransfected with a 1:9 ratio of pcDNA/FRT:pOG44 and selected with hygromycin. Hygromycin-resistant cell clones were picked up and expanded. Target protein expression was verified by immunoblotting. Control cell line was generated by transfecting Flp-In-293 cells with pcDNA5/FRT blank vector containing Flag-HA tags. To generate V15B cells stably expressing Ku80, V15B cells were transfected with plasmid of pcDNA3.1-His-Ku80 using fugene6. The transfectants were selected by zeocin (500 μg/ml) and confirmed by immunoblotting using anti-Ku80 antibody.

Immunoprecipitation and nanoLC/MS/MS

Cells were sonicated in lysis buffer (50 mM Tris–HCl, pH 7.5, 0.15 M NaCl, 0.5% NP-40, 1 mM EDTA) supplemented with protease inhibitor (complete, EDTA-free, Roche). Lysates were incubated on ice in the presence of 20 μg/ml ethidium bromide (EtBr) for 1 h and cleared by centrifugation, and then the supernatants were collected. Immunoprecipitation was carried out with anti-FLAG M2 affinity gel (A2220, Sigma), according to the manufacturer's protocol. Proteins were eluted by lysis buffer containing 100 μg/ml FLAG peptide (F3290, Sigma). Eluted proteins were detected by immunoblotting. For mass spectrometry, a large-scale suspension culture was carried out. Cells were grown in Joklik medium (Sigma) to 1 l kept between 2 and -6×10^5/ml. cells were collected and lysated for immunoprecipitation. Eluted proteins were separated on a 12.5% polyacrylamide gel and stained using a Wako Mass silver stain kit. Gel slippage was reduced by 100 mM DTT and alkylated by 100 mM idoacetamide. After washing, the gels were incubated with trypsin overnight at 30°C. Recovered peptides were desalted by Ziptip c18 (Millipore). Samples were analyzed by nanoLC/MS/MS systems (DiNa HPLC system KYA TECH Corporation/QSTAR XL Applied Biosystems). Mass data acquisitions were piloted by Mascot software (30).

Generation of a stable PHF1 knockdown cell line and colony formation assay

Short hairpin siRNA constructs with 21 ribo-nucleotide sequences from PHF1. Oligo-ribo-nucleotides were synthesized and cloned into the psiRNA-h7SKzeo G1 vector (Invivogen). The PHF1 siRNA vector and control vector (psiRNA-h7SKz-Luc, Invivogen) were transfected into HeLa cells by fuGene6 (Roche). Stable transfectants were selected in the presence of 500 μg/ml zeocin. Knockdown of PHF1 was detected by immunoblotting and real-time PCR. Among the siRNA constructs only one sequence (122-GGACTGATGGGCTGCTATACT) had an effect on the expression of PHF1 in HeLa cell. For the colony formation assay, cells were plated in duplicate at 400 cells/6 cm dishes. Eight hours after plating, cells were irradiated with X-ray. Eight days later, colonies were fixed and stained with 0.3% crystal violet in methanol for counting. Three independent experiments were carried out and the standard errors were indicated with an error bar.

Recombination assay

Recombination assay was carried out as described previously (29). The pCMV3nls-I-sceI expression vector and the HeLa cell line, which contain a stably integrated copy of recombination reporter vector SCneo, were kind gifts from Dr Maria Jasin. Double strand siRNA for PHF1 and scramble were synthesized and purified by a Silencer siRNA construction kit (Ambion) (PHF1: 5′-AA GCTTTCTCTGCCATATGGA. Scramble: 5′-AAGCT TACCGTCTCTTAACGA). The HeLa cells in 3.5 cm dishes were transfected with 2 nM siRNA for PHF1 and control by using OligofectAMINE (Invitrogen). The cells were trypsinized and counted 48 h after transfection. With 2 μg pCMV3nls-I-SceI 1×10^6 cells were electroporated according to manufacturer's protocol (Digital Bio. 950 V, 35 ms and 2 pulse), and cells were plated in 10 cm dishes. Cells were selected in 1 mg/ml of G418 beginning 24 h after electroporation. The cloning efficiency was determined by plating 1000 cells in 10 cm dishes. Colonies were fixed and stained with 0.3% crystal violet in methanol for counting. Three independent experiments were carried out and the standard errors were indicated by an error bar.

Real-time PCR

Total RNA was extracted from cells by using a High Pure RNA Isolation Kit (Roche). cDNA were synthesized by using a First Strand cDNA synthesis Kit (Roche). Real-time PCR was performed in triplicate using Thermal Cycler Dice Real Time System (TaKaRa). The primer of PHF1 used in quantitative PCR were: 5′-TTACTGTTACT GTGGTGGCC, 5′-GGTGATACAGGACAAGATGG.

RESULTS

PHF1 was recruited to DSB sites induced by laser micro-irradiation

We established a laser micro-irradiation system that can induce different types of DNA damage (SSBs, DSBs and base damage) in living cells and have investigated proteins responding to DNA damage (11–13). We found that proteins involved in NHEJ (Ku70, Ku80, XRCC4, Ligase4, XLF and Artemis) and HR factors (Rad52 and NBS1) are recruited to the sites by laser micro-irradiation (Supplementary Figure 1). In an effort to find new components in the cellular process responding to DSBs, we used this system to screen a group of GFP-tagged mouse PcG proteins, which are highly conserved throughout evolution and involved in transcription regulation, development, cell proliferation and tumorigenesis. We found that mPcl1, a component involved in PcG complex PRC2, was recruited to damage site immediately after irradiation with 405 nm laser in the presence of BrdU (data not shown). We observed no recruitment of other PcG proteins including mPcl2, mPcl3, PLZF, Scmh1, Ring1A, Ring1B, Mel18 and EED (data not shown). We isolated a human homolog of mPCl1, PHF1 cDNA, attached it with GFP and expressed in HeLa cell. We found that both endogenous PHF1 and GFP-tagged PHF1 accumulated at the irradiated sites and co-localized with γH2AX or with GFP-tagged Ku70 only after irradiation with 500 scans in the presence of BrdU (Figure 1A and B, see Materials and methods section). Although GFP-PHF1 accumulates at the laser irradiated site after 100 scans with BrdU pretreatment, the accumulation was significantly weak (data not shown). As shown in Figure 1C, GFP-PHF1 accumulates rapidly at the irradiated sites within 1 min after irradiation and dissociates before 10 min. Since PHF1 dissociates very rapidly from DSBs sites, and NHEJ and HR factors remain at damage sites more than 2–4 h after irradiation (data not shown, 22), these data suggest that PHF1 is an early factor involved in DSBs damage response.

PHF1 is recruited to the sites of laser micro irradiation via two independent domains of the N-terminus Tudor domain and the central region

PHF1 contains two zinc finger-like PHD (derived from the name 'plant homeodomain') domains and a Tudor domain (Figure 2A). PHD domain is found in a number of nuclear proteins and thought to be involved in chromatin-mediated transcriptional regulation (23); the Tudor domain is found in several RNA-binding factors and believed to be chromatin-binding domain. To determine which domain is responsible for the recruitment of PHF1 to laser-irradiated sites, we constructed several GFP-tagged PHF1 deletion mutants and analyzed the recruitment of these deletion mutants (Figure 2A). We found that three deletion mutants of PHF1 (aa 2–349, aa 81–431 and aa 340–567) are all recruited to irradiation sites (Figure 2B), suggesting that more than one domain are responsible for the recruitment of PHF1. More detailed analysis showed that both Tudor domain and central region (aa 340–431) are recruited to damaged sites, but PHD domain and C-terminal domain are not (Figure 2B). To further address the importance of Tudor domain and central region (aa 340–431) for the recruitment of PHF1 to laser-irradiated sites, we examined the recruitment of deletion mutants of PHF1 (aa 81–349 and 422–567). As expectedly, deletion mutants of PHF1 (aa 81–349 and 422–567) lacking both Tudor domain and central region (aa 340–431) showed no recruitment to damaged sites (Figure 2B). It has been reported that the two tandem Tudor domains of 53BP1 binds to methylated lysine 79 of histone H3 in response to DNA damage (24,25). Thus, our data show another example that Tudor domain plays an important role in response to DNA damage. Beside Tudor domain, the central region of PHF1 (aa 310–431) is also recruited to laser-irradiated sites, suggesting that PHF1 possesses complexity in response to DNA damage, which is not related to PHD domain.

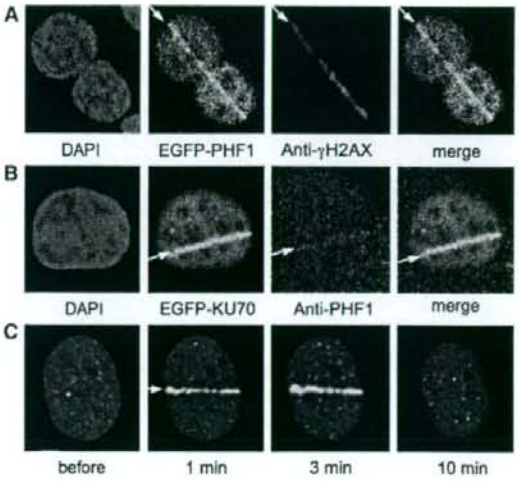

Figure 1. Recruitment of PHF1 to the sites irradiated with 405 nm laser. HeLa cells were sensitized with BrdU and micro-irradiated. Five minutes later, the cells were photographed (for GFP-tagged protein) or fixed and stained with antibody. EGFP-tagged PHF1 is recruited to laser-irradiated sites and co-localizes with γH2AX. (**A**) Accumulation of GFP-tagged PHF1 (EGFP-PHF1) and γH2AX. (**B**) Accumulation of EGFP-KU70 co-localized with endogenous PHF1. (**C**) Accumulation and dissociation of GFP-PHF1 at laser-irradiated sites in HeLa cells. Arrows indicate the sites of irradiation.

Recruitment of PHF1 is Ku70/Ku80 dependent

We tested whether or not the recruitment of PHF1 to laser-irradiated sites is influenced by factors involved in NHEJ or HR. The idea is that, if PHF1 is involved in either NHEJ or HR pathway, its recruitment may be influenced by the absence of upstream factors of either pathway. PHF1 showed normal recruitment in human cell line 1022QVA (Nijmegen patient cells) mutated in NBS1, which is essential for HR (Figure 3D). PHF1 was also recruited to laser-irradiated sites in cells derived

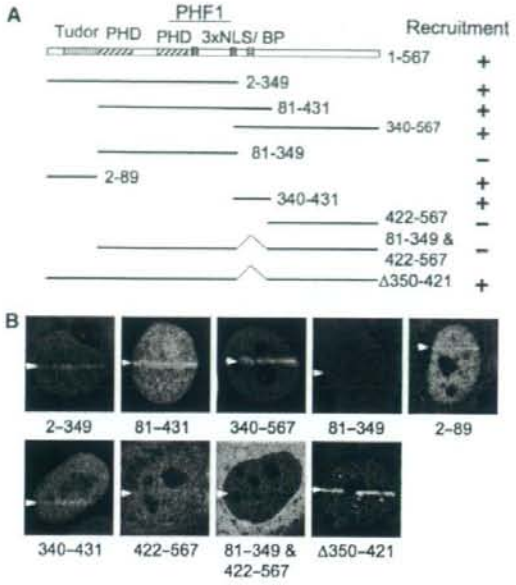

Figure 2. PHF1 is recruited to laser-irradiated sites via two independent domains of the N-terminus Tudor domain and the central region (aa 340–431). (**A**) Schematic presentation of PHF1 domains (top) and deletion mutants (left) and the results of recruitment experiments (right). (**B**) Live cell imaging of irradiated HeLa cells expressing GFP-tagged deletion mutants of PHF1. Arrows indicate the sites of irradiation.

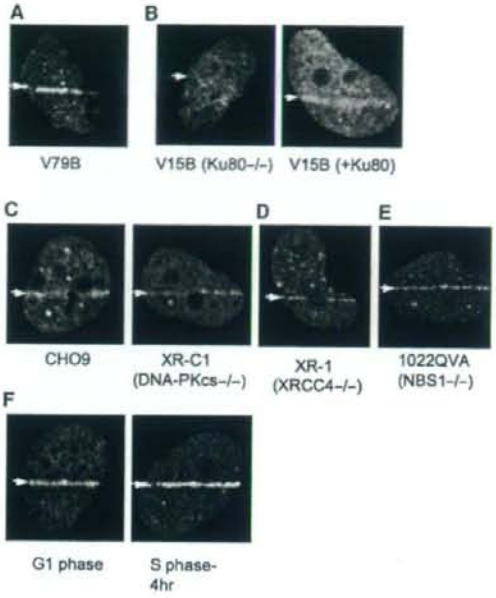

Figure 3. PHF1 is recruited to DSBs in dependence on Ku70/Ku80. (**A**) EGFP-PHF1 accumulates at laser-irradiated site in wild-type V79B. (**B**) EGFP-PHF1 does not accumulate at irradiation sites in V15B cell (Ku80-deficient) but do in V15B cell (+His-Ku80). (**C**) EGFP-PHF1 accumulates at irradiation sites both in DNA-Pkcs-deficient and proficient CHO cells. (**D**) EGFP-PHF1 accumulates at irradiation sites in XR-1 cell (XRCC4-deficient). (**E**) EGFP-PHF1 accumulates at irradiation sites in 1022QVA (NBS1-deficient). (**F**) HeLa cells were synchronized to G1- and G2/S-phase by thymidine and hydroxyurea treatment. PHF1 accumulates at irradiation sites in HeLa cells both in G1 phase and S phase. Arrows indicate the sites of irradiation.

from the Chinese hamster ovary (CHO) cell lines of XR-C1 (DNA-PKcs-deficient), XR-1 (XRCC4-deficient) (Figure 3B and C). However, PHF1 was not recruited to laser-irradiated sites in XR-V15B (Ku80-deficient), while PHF1 is recruited in XR-V79B (Ku80 proficient) (Figure 3A). We generated a V15B cell line expressing His-ku80, in which expression of Ku80 as well as recruitment of Ku70 to laser-irradiated site is restored. In this cell line, recruitment of EGFP-PHF1 is also restored (Figure 3A). Thus, this indicates that PHF1 is recruited to the sites of DSBs in a Ku70/80-dependent manner. Like NHEJ factors, PHF1 is recruited to DSBs sites both in G1 and S/G2 phases (Figure 3E) without cell-cycle dependency.

PHF1 is associated physically with ku70/ku80

Having known that the recruitment of PHF1 is Ku70/Ku80-dependent, we tested whether or not PHF1 is associated with Ku70/Ku80 proteins. In order to check the interaction, we generated two human 293 cell lines stably expressing either PHF1 or Ku80 fusion protein containing FLAG-HA tags. For prevention of any DNA-dependent association, coimmunoprecipitation was carried out in the presence of ethidium bromide (26,27). PHF1 was immunoprecipitated from 293 cells extracts by using anti-FLAG antibody and the immunoprecipitated products were analyzed by western blotting with anti-Ku70 antibody. As shown in Figure 4A, Ku70 was coimmunoprecipitated with Flag-HA-PHF1, but was not present in control immunoprecipitants from the extracts of cells transfected with a blank vector. Moreover, PHF1 also coimmunoprecipitated with FLAG-HA-Ku80 from extracts of cells transfected with FLAG-HA-Ku80, but was not present in control immunoprecipitants (Figure 4B). These results indicate that PHF1 is associated physically with Ku70/Ku80 in the cells.

RNA interference of PHF1 causes cell sensitivity to X-Ray and increases HR frequency

In light of the above data, we speculated that PHF1 might be involved in NHEJ. Either NHEJ or HR deficiency will lead cells to sensitivity to X-Ray or chemical reagent. In order to analyze this, we generated a stable PHF1 knockdown cell line using a vector-based siRNA approach. Characterization of the established cell line indicates that about 77% knockdown is achieved at mRNA level by quantitative RT–PCR (Figure 4C), but only 50% knockdown at the protein level (Figure 4D). Downregulation of PHF1 causes mild cell sensitivity to X-ray (Figure 4E). It is probably due to low efficiency of

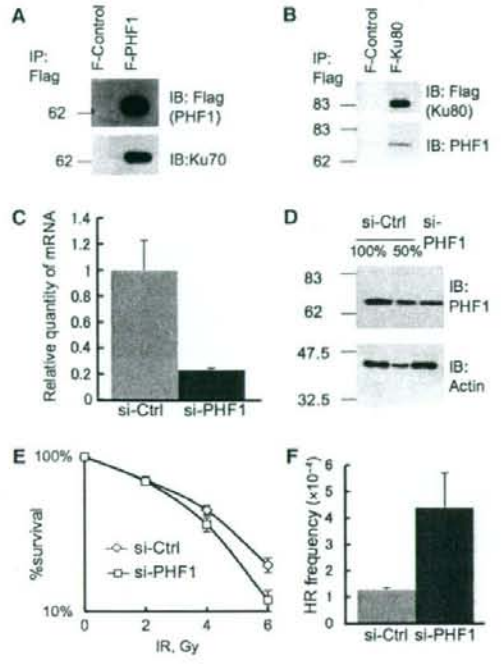

Figure 4. PHF1 is associated physically with Ku70/Ku80 and may be involved in NHEJ. (**A**) pcDNA5/FRT vector expressing FLAG-HA tagged PHF1 was transfected into Flp-In-293 cells, and a clone stably expressing FLAG-HA-PHF1 (F-PHF1) was isolated and used for coimmunoprecipitation by anti-FLAG M2 affinity gel. A clone stably expressing FLAG-HA tag alone (F-Control) was used as negative control. (**B**) pcDNA5/FRT vector expressing FLAG-HA tagged Ku80 was transfected into Flp-In-293 cells, and a clone stably expressing FLAG-HA-PHF1 (F-Ku80) was isolated and used for coimmunoprecipitation by anti-FLAG M2 affinity gel. (**C**) Real-time PCR analysis of a PHF1 stable knockdown cell line and a parallel mock knockdown cell line. HPRT was used as the control for normalization in the real-time PCR. (**D**) Immunoblotting analysis of PHF1 stable knockdown cell line and parallel mock knockdown cell line. Actin serves as a loading control for immunoblotting. (**E**) PHF1 knockdown cell showed increased sensitivity to X-Ray. Cells were plated in 6 cm dishes and irradiated with the indicated doses of ionizing irradiation. (**F**) Recombination frequency in HeLa cells after knockdown of PHF1. Error bars represent standard errors.

PHF1 knockdown. It has been also shown that deficiency in NHEJ components such as Ku70, XRCC4 and DNA-PKcs results in increased levels of HR (28). Therefore, we tested whether or not downregulation of PHF1 affects HR using recombination assay described previously (29). As expectedly, downregulation of PHF1 increases HR frequency several folds (Figure 4F). These data strongly suggest that PHF1 is involved in NHEJ pathway and supports its efficiency.

PHF1 is associated with proteins responding to DNA damage besides KU and those from Polycomb group (PcG)

If PHF1 is involved in damage response besides transcriptional regulation in human cell, PHF1 can be identified in

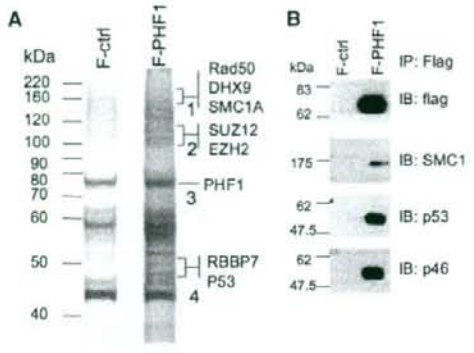

Figure 5. Analysis of PHF1-associated proteins in HeLa cell by proteomics. (**A**) Putative PHF1-binding proteins identified by coimmunoprecipitation and mass spectrometry. Among identified proteins by mass spectrometry, those related to DNA damage response and PcG are indicated. Flp-In-293 cells stably expressing FLAG-HA tagged PHF1 was used for immunoprecipitation for FLAG. Flp-In-293 cells expressing FLAG-HA-tag alone was used as negative control. (**B**) Candidate interacting proteins identified by nanoLC/MS/MS were further confirmed using antibodies against SMC1, p53 and p46 by immunoblotting. Antibodies (IB) are indicated on the right.

a proteome other than PcG group and may have other interacting proteins of damage response than KU. Therefore, a proteomics approach was undertaken to identify interacting proteins of PHF1 within human cell. A 293-cell line stably expressing PHF1 fused with FLAG-HA tags was used to immunoprecipitate the PHF1 complex by anti-FLAG antibody in the presence of ethidium bromide for exclusion of DNA-associated nonspecific proteins. Immunoprecipitated products were analyzed by SDS–PAGE, and then silver stained (Figure 5A); bands were excised, treated as described (30) and tryptic peptides were analyzed by mass spectrometry (Supplementary Table 1). It was not surprising that Suz12, EZH2 and RBBP7 (RbAp46) were identified, consistent with a previous report about *Drosophila* Pcl protein. More interestingly, Rad50, SMC1, DHX9 and P53, which are proteins involved in DNA damage response and repair, were also identified with high confidence as coimmunoprecipitants of PHF1. The data of mass analysis were further confirmed by western blotting with SMC1, p53 and RbAp46 antibodies (Figure 5B). Rad50 forms a complex with Mre11 and NBS1 that is essential in maintaining DNA integrity by functioning in DSBs repair, meiotic recombination and telomere maintenance (31–33).

DISCUSSION

PcG proteins are epigenetic chromatin modifiers involved in gene silencing, cancer development and the maintenance of embryonic and adult stem cells. During screening of proteins responding to DNA damage by using laser micro-irradiation we found that mPcl1, a mouse homolog of polycomb-like protein (Pcl) of the *D. melanogaster*, accumulates at laser-irradiated site. It was previously shown that the *Drosophila* Pcl protein is associated with

a 1 MDa complex containing the members of PcG, ESC, E(Z), SU(Z)12, p55 and RPD3, and, furthermore. Pcl is present in another unknown complex, which does not contain any component of the 600 kDa ESC/E(Z) complex (34). Therefore, we were interested in the mechanisms and function of the damage response and isolated a human homolog of Pcl1, PHF1. PHF1 was identified several years ago as a human homolog of *Drosophila* Pcl that locates on 6p21.3, belonging to MHC classII region (35). Although PHF1 shares significant sequence similarity to the *Drosophila* Pcl, and was shown recently to be involved in tumorigenesis and/or tumor progression of endometrial stromal sarcoma by genetic analysis (36), its function was still unknown. In this study, we identified PHF1 as a new component in DSBs damage response, possibly involved in the repair pathway of DSBs.

Endogenous and GFP-tagged PHF1 were recruited immediately to the sites irradiated with laser micro-irradiation in HeLa cells (Figure 1). Since PHF1 accumulates at the site irradiated with higher laser dose in the presence of BrdU and PHF1 neither accumulates at the site irradiated with lower laser dose of the laser light, nor responds to UV-irradiation (data not shown), PHF1 is possibly involved in DSBs damage response. Although the response of endogenous PHF1 was only weakly shown by antibody (Figure 1), it is probably due to low sensitivity of the antibody and/or rapid dissociation of PHF1 from the accumulated sites as shown by the results obtained with GFP-tagged protein (Figure 1C). PHF1 did not accumulate at irradiated sites in Ku-deficient XR-V15B cells, but it accumulated in V15B cells expressing Ku80 (Figure 3B). These data suggest that PHF1 is recruited under the influence of Ku proteins to DSBs. In contrast to Ku-deficient cells, PHF1 accumulation was not affected in other mutant cells, which are defective in DNA-PKcs, XRCC4 and NBS1 (Figure 3C–E). We thought, therefore, that there might be some physical and/or functional interactions between PHF1 and Ku70/Ku80. Co-IP experiments showed that PHF1 is indeed physically associated with Ku70/Ku80 (Figure 4A and B). In accordance with these data, siRNA-mediated downregulation of PHF1 provided the host HeLa cells with a mild but consistent cell sensitivity to X-ray (Figure 4E). Furthermore, the downregulation of PHF1 leads the cells to an enhanced HR frequency (Figure 4F), which provides further evidence that PHF1 is involved in DSBs repair and supports NHEJ. Like other NHEJ factors PHF1 is recruited to DSBs sites both G1 and S/G2 phases (Figure 3E).

PHF1 contains two zinc finger-like PHD domains and a Tudor domain (Figure 2A). Tudor domain of 53BP1 interacts with methylated histones and mediates its recruitment to DSBs sites (24). Recently, PHD domain was shown to promote both gene expression and repression through an interaction with H3K4me3 tails (37–40). The data reported here showed that PHD domain is not responsible for the recruitment of PHF1 to DSBs sites, while Tudor domain and central region of PHF1 (310–431) are responsible for the recruitment (Figure 2A). Preliminary data suggest that neither of the domains interacts with Ku80 (data not shown) but the whole PHF1 interacts with Ku proteins, suggesting that accumulation of PHF1 at DSBs requires Ku protein and the two domains have individual binding activities to DSBs. Further analysis is necessary to understand the mechanisms behind the recruitment of PHF1 to DSBs.

Besides Ku70/Ku80, PHF1 is also associated with various proteins involved in the response to DSBs and other genomic maintenance mechanisms, Rad50, DHX9, SMC1 and p53 (Figure 5). Rad50 forms a complex with Mre11 and NBS1 that is essential in maintaining DNA integrity by functioning in DSBs repair, meiotic recombination and telomere maintenance (31–33). SMC1 and SMC3 constitute the core of the cohesion complexes which play an important role in the repair of DNA DSBs from yeast to human, and SMC1 and SMC3 also interact with Mre11-Rad50 (41–44). DHX9 is a DNA- and RNA-dependent helicase associated directly with γ-H2AX (45). As a tumor suppressor, p53 plays a central role in the DNA damage response involved in multiple signaling pathways (46,47). Rad50, SMC1 and p53 were also demonstrated to be recruited to DSBs sites induced by laser micro-irradiation (44,48). The SMC1/SMC3 cohesion complex facilitates DSBs repair by HR and holds sister chromatids together locally at DSBs to allow strand invasion and exchange with the sister chromatid template (41–43). Defect in Rad50 influences phosphorylation of SMC1 and reduces HR (31,49). Moreover, another binding protein of PHF1, RbAp46 is a component of histone deacetylase complexes and is involved in chromatin remodeling, interacts with BRCA1 (50). These data suggest that PHF1 may play a role in HR as well. Further analysis is required to understand possible functions of PHF1 in the damage response. While we do not know the exact function of PHF1 in the DSBs repair yet, we demonstrated for the first time in mammalian cells that PHF1, as known as a PcG protein, is involved in DSBs response and possibly in its repair.

SUPPLEMENTARY DATA

Supplementary Data are available at NAR Online.

ACKNOWLEDGEMENTS

We thank Drs Maria Jasin and Hiroshi Tauchi for providing us with expression vector pCMV3nls-I-SceI and HeLa cell line containing a stably integrated copy of recombination reporter vector SCneo. This work was supported in part by a grant from the Genome Network Project, a Grant-in-Aid for Scientific Research (A), 16201010, and Priority Areas Cancer, 18012003 from the Ministry of Education, Culture, Sports, Science and Technology, Japan (to A.Y.). Funding to pay the Open Access publication charges for this article was provided by the Genome Network Projects.

Conflict of interest statement. None declared.

REFERENCES

1. Sonoda,E., Hochegger,H., Saberi,A., Taniguchi,Y. and Takeda,S. (2006) Differential usage of non-homologous

end-joining and homologous recombination in double strand break repair. *DNA Repair*, **5**, 1021–1029.
2. Khanna,K.K. and Jackson,S.P. (2001) DNA double-strand breaks: signaling, repair and the cancer connection. *Nat. Genet.*, **27**, 247–254.
3. Difilippantonio,M.J., Petersen,S., Chen,H.T., Johnson,R., Jasin,M., Kanaar,R., Ried,T. and Nussenzweig,A. (2002) Evidence for replicative repair of DNA double-strand breaks leading to oncogenic translocation and gene amplification. *J. Exp. Med.*, **196**, 469–480.
4. Mills,K.D., Ferguson,D.O. and Alt,F.W. (2003) The role of DNA breaks in genomic instability and tumorigenesis. *Immunol. Rev.*, **194**, 77–95.
5. Valerie,K. and Povirk,L.F. (2003) Regulation and mechanisms of mammalian double-strand break repair. *Oncogene*, **22**, 5792–5812.
6. Sancar,A., Lindsey-Boltz,L.A., Unsal-Kacmaz,K. and Linn,S. (2004) Molecular mechanisms of mammalian DNA repair and the DNA damage checkpoints. *Annu. Rev. Biochem.*, **73**, 39–85.
7. Nussenzweig,A., Chen,C., da Costa Soares,V., Sanchez,M., Sokol,K., Nussenzweig,M.C. and Li,G.C. (1996) Requirement for Ku80 in growth and immunoglobulin V(D)J recombination. *Nature*, **382**, 551–555.
8. Couedel,C., Mills,K.D., Barchi,M., Shen,L., Olshen,A., Johnson,R.D., Nussenzweig,A., Essers,J., Kanaar,R., Li,G.C. *et al.* (2004) Collaboration of homologous recombination and nonhomologous end-joining factors for the survival and integrity of mice and cells. *Genes Dev.*, **18**, 1293–1304.
9. Shiloh,Y. (2003) ATM and related protein kinases: safeguarding genome integrity. *Nat. Rev. Cancer.*, **3**, 155–168.
10. Vidanes,G.M., Bonilla,C.Y. and Toczyski,D.P. (2005) Complicated tails: histone modifications and the DNA damage response. *Cell*, **121**, 973–976.
11. Lan,L., Nakajima,S., Oohata,Y., Takao,M., Okano,S., Masutani,M., Wilson,S.H. and Yasui,A. (2004) In situ analysis of repair processes for oxidative DNA damage in mammalian cells. *Proc. Natl Acad. Sci. USA*, **101**, 13738–13743.
12. Lan,L., Nakajima,S., Komatsu,K., Nussenzweig,A., Shimamoto,A., Oshima,J. and Yasui,A. (2005) Accumulation of Werner protein at DNA double-strand breaks in human cells. *J. Cell Sci.*, **118**, 4153–4162.
13. Hashiguchi,K., Matsumoto,Y. and Yasui,A. (2007) Recruitment of DNA repair synthesis machinery to sites of DNA damage/repair in living human cells. *Nucleic Acids Res.*, **35**, 2913–2923.
14. Orlando,V. (2003) Polycomb, epigenomes, and control of cell identity. *Cell*, **112**, 599–606.
15. Valk-Lingbeek,M.E., Bruggeman,S.W. and van Lohuizen,M. (2004) Stem cells and cancer; the polycomb connection. *Cell*, **118**, 409–418.
16. Sparmann,A. and van Lohuizen,M. (2006) Polycomb silencers control cell fate, development and cancer. *Nat. Rev. Cancer*, **6**, 846–856.
17. Scott,C.L., Gil,J., Hernando,E., Teruya-Feldstein,J., Narita,M., Martinez,D., Visakorpi,T., Mu,D., Cordon-Cardo,C., Peters,G. *et al.* (2007) Role of the chromobox protein CBX7 in lymphomagenesis. *Proc. Natl Acad. Sci. USA*, **104**, 5389–5394.
18. Villa,R., Pasini,D., Gutierrez,A., Morey,L., Occhionorelli,M., Vire,E., Nomdedeu,J.F., Jenuwein,T., Pelicci,P.G., Minucci,S. *et al.* (2007) Role of the polycomb repressive complex 2 in acute promyelocytic leukemia. *Cancer Cell*, **11**, 513–525.
19. Zeidler,M. and Kleer,C.G. (2006) The Polycomb group protein Enhancer of Zeste 2: its links to DNA repair and breast cancer. *J. Mol. Histol.*, **37**, 219–223.
20. Holmes,A.M., Weedmark,K.A. and Gloor,G.B. (2006) Mutations in the extra sex combs and Enhancer of Polycomb genes increase homologous recombination in somatic cells of Drosophila melanogaster. *Genetics*, **172**, 2367–2377.
21. Prasad,R., Liu,Y., Deterding,L.J., Poltoratsky,V.P., Kedar,P.S., Horton,J.K., Kanno,S., Asagoshi,K., Hou,E.W., Khodyreva,S.N. *et al.* (2007) HMGB1 is a cofactor in mammalian base excision repair. *Mol. Cell*, **27**, 829–841.
22. Kim,J.S., Krasieva,T.B., Kurumizaka,H., Chen,D.J., Taylor,A.M. and Yokomori,K. (2005) Independent and sequential recruitment of NHEJ and HR factors to DNA damage sites in mammalian cells. *J. Cell Biol.*, **170**, 341–347.
23. Aasland,R., Gibson,T.J. and Stewart,A.F. (1995) The PHD finger: implications for chromatin-mediated transcriptional regulation. *Trends Biochem. Sci.*, **20**, 56–59.
24. Huyen,Y., Zgheib,O., Ditullio,R.A.Jr, Gorgoulis,V.G., Zacharatos,P., Petty,T.J., Sheston,E.A., Mellert,H.S., Stavridi,E.S. and Halazonetis,T.D. (2004) Methylated lysine 79 of histone H3 targets 53BP1 to DNA double-strand breaks. *Nature*, **432**, 406–411.
25. Du,L.L., Nakamura,T.M. and Russell,P. (2006) Histone modification-dependent and -independent pathways for recruitment of checkpoint protein Crb2 to double-strand breaks. *Genes Dev.*, **20**, 1583–1596.
26. Lai,J.S. and Herr,W. (1992) Ethidium bromide provides a simple tool for identifying genuine DNA-independent protein associations. *Proc. Natl Acad. Sci. USA*, **89**, 6958–6962.
27. Ahnesorg,P., Smith,P. and Jackson,S.P. (2006) XLF interacts with the XRCC4-DNA ligase IV complex to promote DNA nonhomologous end-joining. *Cell*, **124**, 301–313.
28. Pierce,A.J., Hu,P., Han,M., Ellis,N. and Jasin,M. (2001) Ku DNA end-binding protein modulates homologous repair of double-strand breaks in mammalian cells. *Genes Dev.*, **15**, 3237–3242.
29. Johnson,R.D., Liu,N. and Jasin,M. (1999) Mammalian XRCC2 promotes the repair of DNA double-strand breaks by homologous recombination. *Nature*, **401**, 397–399.
30. Kanno,S., Kuzuoka,H., Sasao,S., Hong,Z., Lan,L., Nakajima,S. and Yasui,A. (2007) A novel human AP endonuclease with conserved zinc-finger-like motifs involved in DNA strand break responses. *EMBO J.*, **26**, 2094–2103.
31. Zhong,H., Bryson,A., Eckersdorff,M. and Ferguson,D.O. (2005) Rad50 depletion impacts upon ATR-dependent DNA damage responses. *Hum. Mol. Genet.*, **14**, 2685–2693.
32. Paull,T.T. and Lee,J.H. (2005) The Mre11/Rad50/Nbs1 complex and its role as a DNA double-strand break sensor for ATM. *Cell Cycle*, **4**, 737–740.
33. Lee,J.H. and Paull,T.T. (2005) ATM activation by DNA double-strand breaks through the Mre11-Rad50-Nbs1 complex. *Science*, **308**, 551–554.
34. Tie,F., Prasad-Sinha,J., Birve,A., Rasmuson-Lestander,A. and Harte,P.J. (2003) A 1-megadalton ESC/E(Z) complex from Drosophila that contains polycomblike and RPD3. *Mol. Cell. Biol.*, **23**, 3352–3362.
35. Coulson,M., Robert,S., Eyre,H.J. and Saint,R. (1998) The identification and localization of a human gene with sequence similarity to Polycomblike of Drosophila melanogaster. *Genomics*, **48**, 381–383.
36. Micci,F., Panagopoulos,I., Bjerkehagen,B. and Heim,S. (2006) Consistent rearrangement of chromosomal band 6p21 with generation of fusion genes JAZF1/PHF1 and EPC1/PHF1 in endometrial stromal sarcoma. *Cancer Res.*, **66**, 107–112.
37. Li,H., Ilin,S., Wang,W., Duncan,E.M., Wysocka,J., Allis,C.D. and Patel,D.J. (2006) Molecular basis for site-specific read-out of histone H3K4me3 by the BPTF PHD finger of NURF. *Nature*, **442**, 91–95.
38. Wysocka,J., Swigut,T., Xiao,H., Milne,T.A., Kwon,S.Y., Landry,J., Kauer,M., Tackett,A.J., Chait,B.T., Badenhorst,P. *et al.* (2006) A PHD finger of NURF couples histone H3 lysine 4 trimethylation with chromatin remodelling. *Nature*, **442**, 86–90.
39. Shi,X., Hong,T., Walter,K.L., Ewalt,M., Michishita,E., Hung,T., Carney,D., Pena,P., Lan,F., Kaadige,M.R. *et al.* (2006) ING2 PHD domain links histone H3 lysine 4 methylation to active gene repression. *Nature*, **442**, 96–99.
40. Pena,P.V., Davrazou,F., Shi,X., Walter,K.L., Verkhusha,V.V., Gozani,O., Zhao,R. and Kutateladze,T.G. (2006) Molecular mechanism of histone H3K4me3 recognition by plant homeodomain of ING2. *Nature*, **442**, 100–103.
41. Watrin,E. and Peters,J.M. (2006) Cohesin and DNA damage repair. *Exp. Cell Res.*, **312**, 2687–2693.
42. Potts,P.R., Porteus,M.H. and Yu,H. (2006) Human SMC5/6 complex promotes sister chromatid homologous recombination by recruiting the SMC1/3 cohesin complex to double-strand breaks. *EMBO J.*, **25**, 3377–3388.

43. Losada,A. and Hirano,T. (2005) Dynamic molecular linkers of the genome: the first decade of SMC proteins. *Genes Dev.*, **19**, 1269–1287.
44. Kim,J.S., Krasieva,T.B., LaMorte,V., Taylor,A.M. and Yokomori,K. (2002) Specific recruitment of human cohesin to laser-induced DNA damage. *J. Biol. Chem.*, **277**, 45149–45153.
45. Mischo,H.E., Hemmerich,P., Grosse,F. and Zhang,S. (2005) Actinomycin D induces histone gamma-H2AX foci and complex formation of gamma-H2AX with Ku70 and nuclear DNA helicase II. *J. Biol. Chem.*, **280**, 9586–9594.
46. Helton,E.S. and Chen,X. (2007) p53 modulation of the DNA damage response. *J. Cell Biochem.*, **100**, 883–896.
47. Su,T.T. (2006) Cellular responses to DNA damage: one signal, multiple choices. *Annu. Rev. Genet.*, **40**, 187–208.
48. Bekker-Jensen,S., Lukas,C., Kitagawa,R., Melander,F., Kastan,M.B., Bartek,J. and Lukas,J. (2006) Spatial organization of the mammalian genome surveillance machinery in response to DNA strand breaks. *J. Cell Biol.*, **173**, 195–206.
49. Gorski,M.M., Romeijn,R.J., Eeken,J.C., de Jong,A.W., van Veen,B.L., Szuhai,K., Mullenders,L.H., Ferro,W. and Pastink,A. (2004) Disruption of Drosophila Rad50 causes pupal lethality, the accumulation of DNA double-strand breaks and the induction of apoptosis in third instar larvae. *DNA Repair*, **3**, 603–615.
50. Yarden,R.I. and Brody,L.C. (1999) BRCA1 interacts with components of the histone deacetylase complex. *Proc. Natl Acad. Sci. USA*, **96**, 4983–4988.

A Lysosomal Protein Negatively Regulates Surface T Cell Antigen Receptor Expression by Promoting CD3ζ-Chain Degradation

Rika Ouchida,[1] Sho Yamasaki,[2] Masaki Hikida,[3] Keiji Masuda,[1] Kiyoko Kawamura,[5] Akihiko Wada,[5] Shigenobu Mochizuki,[5] Masatoshi Tagawa,[5] Akemi Sakamoto,[6] Masahiko Hatano,[6] Takeshi Tokuhisa,[6] Haruhiko Koseki,[4] Takashi Saito,[2] Tomohiro Kurosaki,[3] and Ji-Yang Wang[1,*]

[1]Laboratory for Immune Diversity
[2]Laboratory for Cell Signaling
[3]Laboratory for Lymphocyte Differentiation
[4]Laboratory for Developmental Genetics
Research Center for Allergy and Immunology, RIKEN Yokohama Institute, Yokohama 230-0045, Japan
[5]Division of Pathology, Chiba Cancer Center Research Institute, Chiba 260-8717, Japan
[6]Department of Developmental Genetics, Graduate School of Medicine, Chiba University, Chiba 260-8670, Japan
*Correspondence: oh@rcai.riken.jp
DOI 10.1016/j.immuni.2008.04.024

SUMMARY

Modulation of surface T cell antigen receptor (TCR) expression is an important mechanism for the regulation of immune responses and the prevention of T cell hyperactivation and autoimmunity. The TCR is rapidly internalized after antigen stimulation and then degraded in lysosomes. However, few of the molecules involved in this process have been identified. We demonstrate that the lysosomal protein LAPTM5 negatively regulated surface TCR expression by specifically interacting with the invariant signal-transducing CD3ζ chain and promoting its degradation without affecting other CD3 proteins, CD3ε, CD3δ, or CD3γ. TCR downmodulation required the polyproline-tyrosine motifs and the ubiquitin-interacting motif of LAPTM5. LAPTM5 deficiency resulted in elevated TCR expression on both CD4$^+$CD8$^+$ thymocytes and spleen T cells after CD3 stimulation, as well as enhanced T cell responses in vitro and in vivo. These results identify a lysosomal protein important for CD3ζ degradation and illustrate a unique mechanism for the control of surface TCR expression and T cell activation.

INTRODUCTION

The T cell antigen receptor (TCR) is a multisubunit complex composed of the variable antigen-binding TCR αβ or γδ chains noncovalently associated with the invariant signal-transducing CD3γε, CD3δε, and CD3ζζ (TCRζ, CD247) chains (Kuhns et al., 2006). TCR signaling is dynamic and regulated by multiple mechanisms to ensure that appropriate signals are delivered during T cell development and to control effector functions of mature T cells. One important mechanism for the regulation of TCR signal strength is the modulation of its cell-surface expression (Viola and Lanzavecchia, 1996). During T cell development in the thymus, surface TCR is maintained at low amounts at the CD4$^+$8$^+$ double-positive (DP) stage, presumably to allow for optimal positive and negative selection, and is upregulated in CD4$^+$ and CD8$^+$ single-positive (SP) cells that have undergone selection (Schrum et al., 2003). In the periphery, the TCR on mature T cells is rapidly downmodulated upon antigen stimulation. This downregulation is a critical process for the termination of signal transduction and the prevention of T cell hyperactivation and autoimmunity (Naramura et al., 2002).

The TCR undergoes constitutive internalization and is then either recycled back to the plasma membrane or sorted to lysosomes for degradation (Liu et al., 2000; Geisler, 2004; von Essen et al., 2004; Valitutti et al., 1997). Modification of any of these processes would affect steady-state TCR expression on the cell surface (Liu et al., 2000; Geisler, 2004). Similar processes occur after TCR triggering, but the kinetics is more rapid. In DP thymocytes, the Src-like adaptor protein (SLAP) (Sosinowski et al., 2000, 2001) and the RING-type E3 ubiquitin ligase Casitas B lineage lymphoma (c-Cbl) (Naramura et al., 1998; Murphy et al., 1998) function to promote the degradation of the internalized TCR. SLAP and c-Cbl together target CD3ζ for ubiquitination and degradation and thereby prevent the accumulation of fully assembled recycling TCR (Wang et al., 2001; Myers et al., 2005, 2006). Deficiency of SLAP and/or c-Cbl results in elevated surface TCR expression in DP thymocytes and enhanced positive selection of thymocytes expressing an MHC class II-restricted TCR (Sosinowski et al., 2001; Naramura et al., 1998). In mature T cells, another Cbl family protein, Cbl-b, plays a critical role in negatively regulating T cell activation (Bachmaier et al., 2000; Chiang et al., 2000) and in the downmodulation of surface TCR after CD3 stimulation (Naramura et al., 2002). Cbl-b, together with c-Cbl, functions to direct the internalized TCR to the lysosomal compartment for degradation by an as-yet-unknown mechanism (Naramura et al., 2002). T cells lacking both Cbl-b and c-Cbl are impaired in ligand-induced TCR downmodulation and exhibit greatly enhanced responses to CD3 stimulation.

TCR complexes are assembled in the endoplasmic reticulum in a step-wise fashion, with the association of CD3ζ homodimer as the final step (Call and Wucherpfennig, 2005). Although all of the TCR components are required for the full assembly of the TCR complex and its transport to the plasma membrane, CD3ζ can be a limiting factor that determines the surface expression of the TCR. For example, surface TCR expression in 2B4 T cells correlated quantitatively with CD3ζ protein amounts (D'Oro et al., 2002). Very recently, it was found that deficiency of CD3ζ in humans caused severe combined immunodeficiency by preventing normal TCR assembly and surface expression (Rieux-Laucat et al., 2006; Roberts et al., 2007). In addition to its pivotal role in regulating the assembly of newly synthesized TCR complexes, the fate of CD3ζ after TCR internalization appears to determine the destiny of the entire TCR complex, i.e., recycling or degradation. SLAP-deficient DP thymocytes expressed increased amounts of CD3ζ, but not TCRα, TCRβ or CD3ε, and elevated surface TCR expression as compared with wild-type DP thymocytes (Myers et al., 2005), indicating that the surface TCR expression in DP thymocytes is dependent on CD3ζ expression. Conversely, forced expression of SLAP and c-Cbl in Jurkat T cells resulted in decreased surface TCR, and the ability of various SLAP and c-Cbl mutants to downregulate surface TCR correlated with their ability to induce CD3ζ degradation (Myers et al., 2006). Together, these observations demonstrate that CD3ζ is an important component that regulates surface TCR expression and T cell function. It remains largely unclear, however, how CD3ζ is targeted to the lysosomes and whether any lysosomal proteins are involved in its degradation.

During the course of identifying genes whose expression was downregulated upon B and T cell activation, we previously isolated a mouse gene and named it *Clast6* (for CD40-ligand-activated specific transcripts) (Seimiya et al., 2003). *Clast6* turned out to be identical to the hematopoietic-specific genes *LAPTM5* and *Laptm5*, identified in human and mouse, respectively (Adra et al., 1996; Scott et al., 1996). LAPTM5 is a lysosomal protein that contains five membrane-spanning segments, three polyproline-tyrosine (PY) motifs (L/PPxY), which are known to bind WW domains involved in protein-protein interactions, and a ubiquitin-interacting motif (LxxALxxSxxE) in the C terminus (Adra et al., 1996; Hofmann and Falquet, 2001; Pak et al., 2006). In a separate expression-cloning approach to identify genes that are involved in TCR signaling, we also isolated a 294 bp fragment that encoded the 98 N-terminal amino acids of LAPTM5. When fused with the extracellular domain of CD8, this short peptide induced NF-AT activation in response to CD8 crosslinking, suggesting a role for LAPTM5 in regulating T cell activation (unpublished data). To explore its physiological role in the immune system, here we have generated and analyzed *Laptm5*-gene-targeted mice. Our results demonstrate that LAPTM5 negatively regulates TCR signaling by promoting CD3ζ degradation.

RESULTS

Generation of LAPTM5-Deficient Mice

Laptm5 is preferentially expressed in lymphoid tissues and transiently downregulated upon T and B cell activation (Figure S1 available online). We therefore employed a conventional approach to inactivate the *Laptm5* gene. We designed a targeting vector to replace the first exon, which contains the translational initiation codon, and 859 bp of the promoter region, with a neo gene (Figures S2A and S2B). Homologous recombination in Bruce4 embryonic stem cells (ESCs) was verified by long-range genomic PCR analysis with primers flanking the 5′ (s157459) and 3′ (as169968) arms and neo primers (neos and neoas) (Figures S2B and S2C). The neo insertion and the genotypes of the gene-targeted mice were monitored by genomic PCR (Figure S2D). Immunoblot analysis revealed LAPTM5 protein expression in wild-type but not *Laptm5*$^{-/-}$ thymocytes (Figure S2E). To further verify the lack of LAPTM5 protein expression in the *Laptm5*$^{-/-}$ mice, we performed immunocytological staining of purified spleen T cells. Punctate LAPTM5 staining was clearly evident in the cytoplasm of wild-type but not *Laptm5*$^{-/-}$ T cells (Figure S2F). These results demonstrate the successful inactivation of the *Laptm5* gene.

Laptm5$^{-/-}$ T Cells Exhibit Elevated Responses to CD3 Stimulation

Fluorescence-activated cell sorting (FACS) analysis of bone marrow, thymus, and spleen cells from more than seven pairs of wild-type and *Laptm5*$^{-/-}$ mice showed no evident differences in the B and T cell populations (Figure S3), indicating that LAPTM5 deficiency had no effect on lymphocyte development and maturation. We next examined lymphocyte function by analyzing the proliferative responses of purified B and T cells to various activation signals in vitro. B cells responded normally to different doses of IgM antibodies, CD40 ligand, and lipopolysaccharide (LPS) (Figure S4). However, splenic T cells consistently exhibited increased proliferation, as measured by [^{3}H] thymidine uptake (Figure 1A), and elevated production of IL-2 and IFN-γ (Figure 1B) in response to CD3 stimulation as compared with wild-type T cells. To examine the response of individual T cells, we analyzed cell division by a carboxyfluorescein diacetate succinimidyl ester (CFSE) assay and cytokine production by intracellular staining. *Laptm5*$^{-/-}$ T cells underwent more cell divisions (Figure 1C, left panel) and a larger fraction of the cells expressed IFN-γ (Figure 1C, right panel) compared with wild-type T cells (wild-type, 11.5% ± 1.7%; *Laptm5*$^{-/-}$, 18.2% ± 1.0%, $p < 0.05$), consistent with the increased [^{3}H] thymidine uptake and cytokine secretion observed at the population level. However, the intracellular levels of IFN-γ on a per-cell basis were increased only marginally in *Laptm5*$^{-/-}$ T cells (mean fluorescence intensity: wild-type, 55.2 ± 4.6; *Laptm5*$^{-/-}$, 68.3 ± 9.3; $p > 0.2$; Figure 1C, right panels), indicating that the maximum response of individual cells was not significantly enhanced in *Laptm5*$^{-/-}$ T cells. Therefore, the increased proliferation and cytokine production in *Laptm5*$^{-/-}$ T cells are more likely due to sustained activation rather than hyperactivation of individual cells. To investigate whether the elevated proliferation was due to increased IL-2 production, we first examined CD3-mediated proliferation in the presence of different doses of IL-2. The exogenously added IL-2 increased proliferation in both wild-type and *Laptm5*$^{-/-}$ T cells, although the enhancing effect plateaued at about 10 U/ml of IL-2 (Figure 1D, left panel). Even at high doses of IL-2, *Laptm5*$^{-/-}$ T cells still exhibited elevated proliferation after CD3 stimulation, indicating that the enhanced proliferation was not an indirect effect of increased IL-2 production. In keeping with that interpretation, *Laptm5*$^{-/-}$ T cells responded to CD3

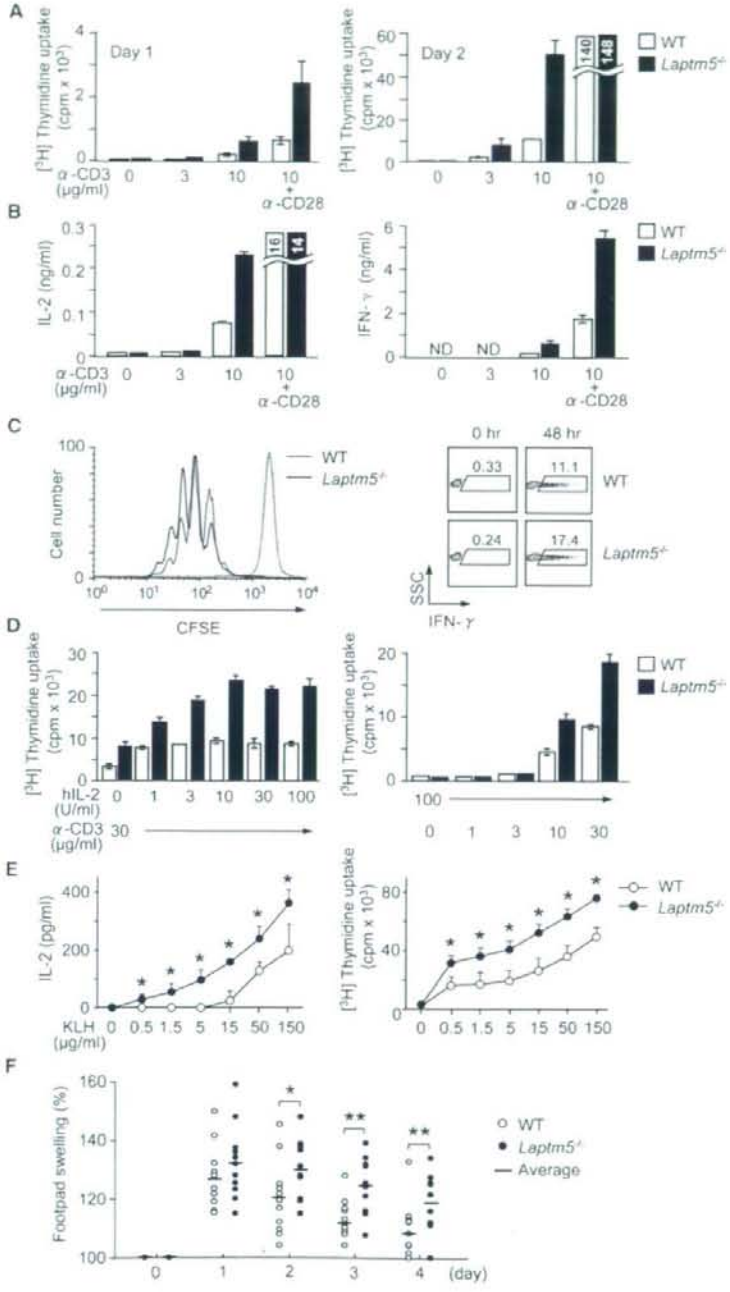

Figure 1. Enhanced T Cell Responses In Vitro and In Vivo in *Laptm5*$^{-/-}$ Mice

(A) Proliferation. Purified spleen T cells (5 × 10^4/well in 96-well plates) were stimulated with plate-bound anti-CD3 with or without anti-CD28 costimulation for 1 and 2 days, and T cell proliferation was analyzed by [^{3}H] thymidine uptake. Mean ± SD is shown. The response of *Laptm5*$^{-/-}$ T cells plateaued on day 2, when stimulated with both anti-CD3 and anti-CD28. Similar results were obtained in six independent experiments.

(B) Cytokine production. Spleen T cells were stimulated as in (A) for 2 days, and amount of IL-2 (left panel) and IFN-γ (right panel) in the supernatant was measured by ELISA. Data are presented as mean ± SD, and similar results were obtained in three independent experiments.

(C) Increase in cell division and numbers of cytokine-producing cells after CD3 stimulation of *Laptm5*$^{-/-}$ T cells. Left panel: cell division as measured by a CFSE assay; right panel: intracellular staining of IFN-γ. Cells were stimulated with plate-bound anti-CD3 (10 μg/ml) for 2 days. The experiments were repeated twice with similar results.

(D) Elevated CD3 responses of *Laptm5*$^{-/-}$ T cells are independent of IL-2. Left panel: responses to CD3 stimulation in the presence of different concentrations of IL-2; right panel: responses to different amounts of CD3 stimulation in the presence of excess IL-2. Cells were stimulated for 1 day and analyzed by [^{3}H] thymidine uptake. Similar results were obtained in three independent experiments.

(E) Recall response of in vivo-activated T cells. Mice (seven wild-type and seven *Laptm5*$^{-/-}$ mice) were immunized with KLH in CFA intradermally in both hind footpads, and 1 week after the immunization, cells of popliteal draining lymph nodes from each mouse were stimulated with different doses of KLH for 3 days. Left panel: IL-2 production; right panel: cell proliferation as measured by [^{3}H] thymidine uptake. Data are presented as mean ± SD; *, $p < 0.05$ (unpaired t test).

(F) Delayed-type hypersensitivity. Mice (12 wild-type and 12 *Laptm5*$^{-/-}$ mice) were sensitized subcutaneously with mBSA in CFA. One week after the sensitization, mice were challenged with the same antigen, and the footpad swelling was measured. *, $p < 0.05$; **, $p < 0.01$ (unpaired t test).

stimulation better than wild-type T cells in the presence of excess IL-2 (Figure 1D, right panel). These results demonstrate that *Laptm5*$^{-/-}$ T cells are hypersensitive to TCR signaling.

Enhanced In Vivo T Cell Responses in *Laptm5*$^{-/-}$ Mice

As a first approach to determining the in vivo effects of LAPTM5 deficiency, we examined T cell responsiveness in an ex vivo assay. Mice were immunized with keyhole limpet hemocyanin (KLH) in complete Freund's adjuvant (CFA) intradermally in both hind footpads. One week after immunization, whole lymph node cells were prepared from the draining popliteal lymph nodes and stimulated with different doses of KLH. *Laptm5*$^{-/-}$ cells exhibited significantly elevated IL-2 production (Figure 1E, left panel) and

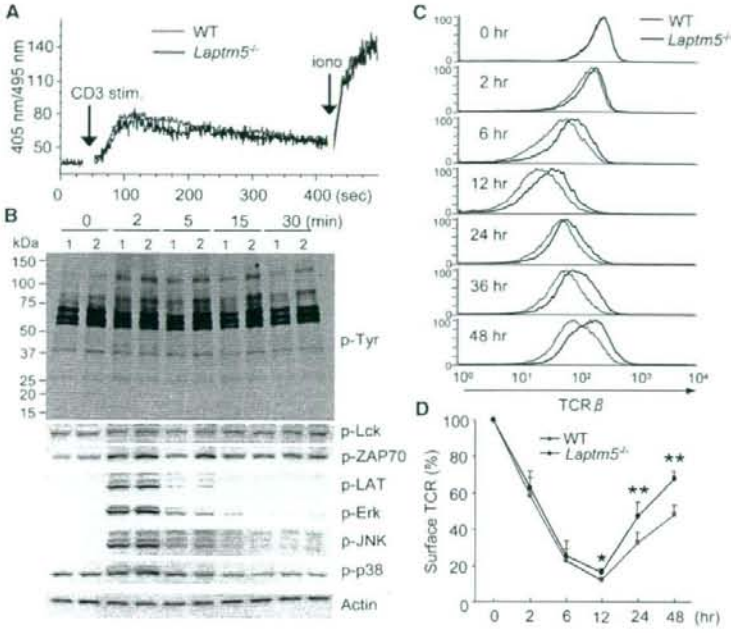

Figure 2. Reduced TCR Downmodulation in *Laptm5*$^{-/-}$ Spleen T Cells after CD3 Stimulation

(A) Normal Ca^{2+} influx in response to CD3 cross-linking in *Laptm5*$^{-/-}$ T cells.

(B) Upper panel: overall tyrosine phosphorylation induced by CD3 stimulation in wild-type (lane 1) and *Laptm5*$^{-/-}$ (lane 2) T cells. Lower panels: phosphorylation of molecules involved in T cell activation.

(C) TCR downmodulation after CD3 stimulation. Spleen T cells were stimulated with plate-bound anti-CD3 and analyzed for surface TCR expression at the indicated time points. A representative FACS profile is shown.

(D) TCR downmodulation in wild-type and *Laptm5*$^{-/-}$ T cells stimulated with anti-CD3. Average ± SD of seven independent experiments is shown. *, $p < 0.05$; **, $p < 0.01$ (unpaired t test).

enhanced proliferation (right panel), indicating that *Laptm5*$^{-/-}$ T cells expanded more efficiently and/or responded more vigorously in vivo than wild-type T cells.

We next examined delayed-type hypersensitivity (DTH), an immune response mediated primarily by $CD4^+$ T cells. Mice were sensitized subcutaneously with methylated bovine serum albumin (BSA) in complete Freund's adjuvant (CFA). Seven days after the sensitization, mice were challenged with the same antigen in one footpad, and the footpad swelling was measured. Both wild-type and *Laptm5*$^{-/-}$ mice exhibited a similar increase in footpad swelling on day 1 after antigen challenge (Figure 1F). However, the footpad swelling quickly subsided in wild-type mice, but persisted in *Laptm5*$^{-/-}$ mice (Figure 1F), indicating that *Laptm5*$^{-/-}$ T cells had an abnormally prolonged response to antigen stimulation.

Reduced TCR Downmodulation in *Laptm5*$^{-/-}$ T Cells

To explore the mechanism for the hyperresponsiveness to CD3-mediated signaling, we first compared cell-surface TCR expression between wild-type and *Laptm5*$^{-/-}$ spleen T cells and found no differences (Figure 2C, 0 hr) indicating that this phenotype was not due to increased expression of the TCR in *Laptm5*$^{-/-}$ T cells. In addition, wild-type and *Laptm5*$^{-/-}$ T cells exhibited a similar Ca^{2+} response after CD3 stimulation (Figure 2A), suggesting that early signaling events, including the activation of PLC-γ1 that is essential for Ca^{2+} mobilization, were not enhanced in the absence of LAPTM5. Consistent with the normal Ca^{2+} response, CD3 stimulation of wild-type and *Laptm5*$^{-/-}$ T cells induced a similar magnitude and pattern in both the overall protein tyrosine phosphorylation and the phosphorylation of specific molecules known to be involved in TCR signaling, including Lck, ZAP70, LAT, Erk, JNK, and p38 (Figure 2B).

The relatively normal early signaling events but enhanced proliferation and cytokine production in *Laptm5*$^{-/-}$ T cells suggested that TCR signaling may not be appropriately terminated. One potential mechanism to turn off TCR signaling is by receptor downmodulation. We therefore analyzed anti-CD3-induced TCR downmodulation and re-expression. Splenocytes were stimulated with plate-bound anti-CD3, and the TCR was examined by flow cytometry. As shown in Figure 2C, cell-surface TCR was downregulated by CD3 stimulation both in wild-type and *Laptm5*$^{-/-}$ T cells. After 6 hr of stimulation, however, *Laptm5*$^{-/-}$ T cells expressed higher amounts of cell-surface TCR. This increase in the TCR expression persisted at 12 hr and 24 hr, and even at 48 hr, after stimulation. The increased expression of TCR was consistently observed in seven independent experiments (Figure 2D). These results demonstrate that *Laptm5*$^{-/-}$ T cells respond normally during the immediate early phase of CD3 stimulation but exhibit prolonged responses, probably as a result of reduced downmodulation of the TCR.

Reduced Degradation of CD3ζ in *Laptm5*$^{-/-}$ T Cells

The higher expression of surface TCR in *Laptm5*$^{-/-}$ T cells relative to wild-type T cells after CD3 stimulation could be due to impaired TCR internalization, enhanced recycling of the internalized TCR back to cell surface, or impaired TCR degradation. To distinguish among these possibilities, we first examined TCR internalization and found that *Laptm5*$^{-/-}$ T cells internalized TCR with exactly the same kinetics as wild-type T cells (Figure 3A). In addition, *Laptm5*$^{-/-}$ T cells showed no evidence of enhanced recycling of the internalized TCR (Figure 3B). These results suggest that the elevated TCR expression observed in *Laptm5*$^{-/-}$ T cells after CD3 stimulation could be due to impaired degradation of the internalized TCR.

The TCR has been shown to be degraded in lysosomes, and the lysosomal localization of LAPTM5 is consistent with

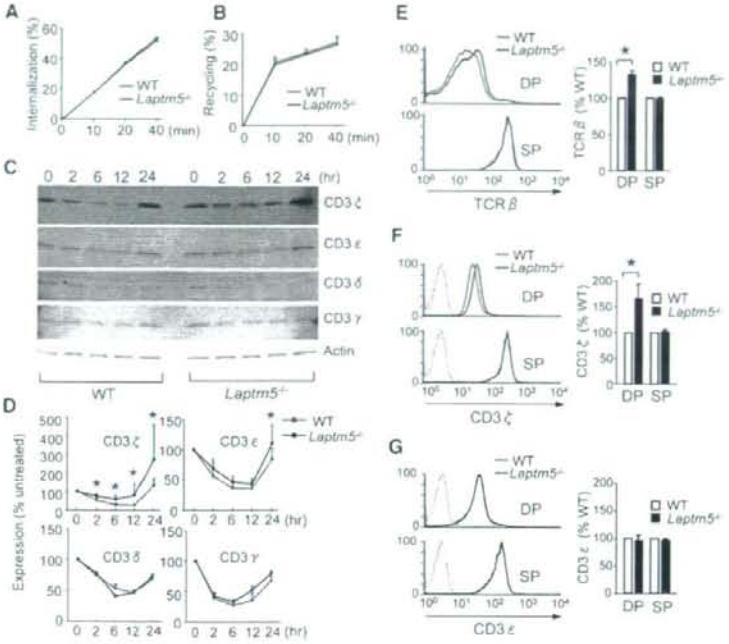

Figure 3. Reduced CD3ζ degradation in *Laptm5*$^{-/-}$ T cells

(A and B) Normal TCR internalization after CD3 stimulation in *Laptm5*$^{-/-}$ T cells (A), and normal recycling of the internalized TCR (B). Mean ± SD of two independent experiments are shown.

(C) Reduced CD3ζ degradation in *Laptm5*$^{-/-}$ T cells stimulated with plate-bound anti-CD3.

(D) Degradation of CD3ζ, CD3ε, CD3δ, and CD3γ. The results of seven independent experiments are shown. *, $p < 0.05$ (unpaired t test).

(E–G) Elevated expression of cell-surface TCR and total amounts of cellular CD3ζ in DP thymocytes of *Laptm5*$^{-/-}$ mice. Surface expression of TCR (E), total cellular amounts of CD3ζ (F) and CD3ε (G) in DP and SP thymocytes of WT and *Laptm5*$^{-/-}$ mice are shown. Left panels: typical FACS profiles; right panels: average ± SD of the results from seven pairs of wild-type and *Laptm5*$^{-/-}$ mice. *, $p < 0.0001$ (unpaired t test).

a possible role in TCR degradation. Because CD3ζ is a critical component in TCR metabolism, we examined its degradation in spleen T cells after stimulation with plate-bound anti-CD3. CD3ζ protein levels decreased both in wild-type and *Laptm5*$^{-/-}$ T cells and reached the lowest levels at 12 hr after stimulation. However, *Laptm5*$^{-/-}$ T cells expressed slightly higher amounts of CD3ζ compared with wild-type T cells (Figure 3C), suggesting that CD3ζ degradation was reduced. The reduction in protein degradation appeared to be CD3ζ-specific because the expression of CD3ε, CD3δ, and CD3γ decreased with a similar kinetics in wild-type and *Laptm5*$^{-/-}$ T cells (Figure 3C). Similar results were obtained in seven independent experiments (Figure 3D).

An increase in CD3ζ protein expression has been observed in DP thymocytes lacking either c-Cbl or SLAP, and in both cases there was elevated cell-surface TCR on CD4$^+$CD8$^+$ DP but not CD4$^+$ or CD8$^+$ SP thymocytes (Sosinowski et al., 2001; Naramura et al., 1998; Myers et al., 2005, 2006). We therefore first compared cell-surface TCR expression on thymocyte subpopulations between wild-type and *Laptm5*$^{-/-}$ mice. We have examined seven pairs of wild-type and *Laptm5*$^{-/-}$ mice, and in every case we observed a small but consistent increase in cell-surface TCR on *Laptm5*$^{-/-}$ DP but not SP thymocytes (Figure 3E). As was the case for c-Cbl or SLAP deficiency, *Laptm5*$^{-/-}$ DP thymocytes expressed increased amounts of total cellular CD3ζ (Figure 3F). In contrast, there was no difference in the amount of CD3ε between wild-type and *Laptm5*$^{-/-}$ DP thymocytes (Figure 3G), indicating that LAPTM5 deficiency specifically affected the protein expression of CD3ζ at the DP stage of thymocyte differentiation. These results demonstrate that LAPTM5 is involved in CD3ζ degradation both in anti-CD3-stimulated spleen T cells and in DP thymocytes.

LAPTM5 Downmodulates Surface TCR by Promoting the Degradation of CD3ζ

To obtain direct evidence for LAPTM5-mediated CD3ζ degradation, we next performed a series of experiments in 2B4 T cells. Previous studies have demonstrated that cell-surface TCR expression in 2B4 cells is quantitatively dependent on the amounts of CD3ζ (D'Oro et al., 2002). We transduced 2B4 cells with retrovirus expressing LAPTM5-IRES-GFP (LAPTM5) or IRES-GFP alone (GFP) as a control and sorted the GFP-positive population. FACS analysis revealed reduced surface TCR expression (Figure 4A, left panel), and immunoblot analysis demonstrated an ~50% reduction in CD3ζ protein amounts (Figure 4A, right panel) in cells expressing LAPTM5 as compared with cells expressing GFP. Notably, the amount of the CD3ε was unaffected by LAPTM5 expression (Figure 4A, right panel), demonstrating that LAPTM5 in T cells specifically targets the endogenous CD3ζ for degradation.

We further examined cytokine production by 2B4 cells expressing LAPTM5 or GFP. Remarkably, IL-2 production induced by CD3 stimulation was strongly inhibited in 2B4 cells expressing LAPTM5 (Figure 4B, left panel). This profound inhibition of cytokine production was specific to TCR-mediated signaling because PMA plus ionomycin induced a similar amount of IL-2 in both transductants (Figure 4B, right panel). In addition, introduction of exogenous CD3ζ restored both surface TCR (Figure S5A) and T cell response to CD3 stimulation (Figure S5B) in LAPTM5-expressing 2B4 cells, demonstrating that LAPTM5 downmodulates surface TCR and inhibits TCR signaling by targeting CD3ζ for degradation.

To ensure that the results obtained in 2B4 T cells were not a cell-line artifact, we further analyzed LAPTM5-mediated TCR downmodulation in normal spleen T cells (Figure 4C). We first stimulated T cells for 24 hr with plate-bound anti-CD3 plus anti-CD28. This treatment induced rapid cell division and allowed us to simultaneously transduce two different retroviruses expressing either LAPTM5-IRES-hCD8 or CD3ζ-IRES-GFP.

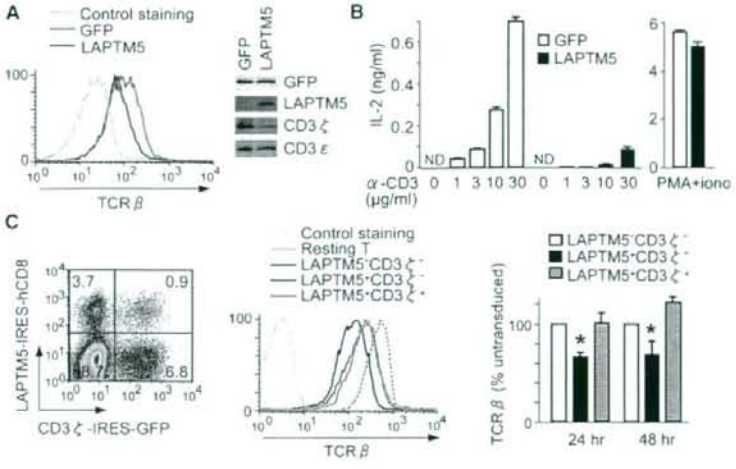

Figure 4. LAPTM5 Downregulates Surface TCR by Promoting the Degradation of CD3ζ Chain

(A) Left panel: surface TCR expression in 2B4 cells expressing GFP (orange line) or LAPTM5 (blue line); right panel: the protein amounts of endogenous CD3ζ and CD3ε in 2B4 cells expressing GFP or LAPTM5. (B) 2B4 cells expressing GFP or LAPTM5 were stimulated for 1 day with plate-bound anti-CD3 (left panel) or with PMA plus ionomycin (right panel), and the amount of IL-2 in the culture supernatant was measured. (C) Normal spleen T cells were transduced with retrovirus expressing either LAPTM5-IRES-hCD8 or CD3ζ-IRES-GFP and analyzed for surface TCR expression. Left panel: FACS profile of virus-transduced spleen T cells; middle panel: surface TCR expression on gated cell population; right panel: average ± SD of three independent experiments. *, $p < 0.05$ when compared to untransduced cells or to cells expressing both LAPTM5 and CD3ζ (unpaired t test).

After retroviral transduction, the cells were further cultured in the presence of plate-bound anti-CD3 for 24 or 48 hr and then analyzed for cell-surface TCR expression on the gated population. Cells that were not transduced with either virus (LAPTM5$^-$CD3ζ$^-$, 88.7%) expressed reduced amounts of surface TCR (orange line, middle panel) as compared to uncultured resting T cells (dotted line), which represented normal TCR downmodulation induced by CD3 stimulation. Cells transduced with LAPTM5 alone (LAPTM5$^+$CD3ζ$^-$, 3.7%) further downmodulated their surface TCR (blue line, middle panel) when compared to nontransduced cells (orange line). This further downmodulation, however, was completely restored by coexpression of CD3ζ (LAPTM5$^+$CD3ζ$^+$, green line). Similar results were obtained in two additional independent experiments, and the average TCR expression (± standard deviation [SD]) is shown in Figure 4C (right panel). These results provide compelling evidence that LAPTM5 downmodulates surface TCR by targeting CD3ζ for degradation both in a T cell hybridoma and in normal spleen T cells.

TCR Downmodulation Requires the PY Motifs and the UIM of LAPTM5

To determine which domains of LAPTM5 are needed to downmodulate surface TCR, we generated a series of LAPTM5-IRES-GFP constructs (Figure S6A) and transduced into 2B4 cells. Surface TCR expression was analyzed on GFP$^+$ versus GFP$^-$ cells by flow cytometry (Figure S6B). Whereas mutation of the first PY motif (mPY1) did not affect the function of LAPTM5, mutation of the third PY motif (mPY3) eliminated the ability of LAPTM5 to downmodulate TCR (Figure 5A). Mutation of the second PY motif (mPY2) also abolished the ability to downmodulate TCR. However, because mPY2 was poorly expressed in 2B4 cells (Figure 5B), it is unclear whether the lack of TCR downmodulation was solely attributable to the lack of PY2 motif. It should be noted that the mPY2 mutant as well as other constructs could be efficiently expressed in 293T cells (not shown). Mutation of the ubiquitin-interacting motif (mUIM) also decreased the ability of LAPTM5 to downmodulate TCR (Figure 5A). Unexpectedly, when the three PY motifs were all mutated (mPY1-3) and expressed in 2B4, not only was surface TCR not downmodulated, but instead it was upregulated three times as much as that on wild-type 2B4 cells (Figure 5A). These observations suggest the possibility that mPY1-3 mutant may function as a dominant-negative protein that interferes with additional pathways of TCR downmodulation.

LAPTM5 and CD3ζ Interact and Colocalize in Lysosomes

Because lysosomal activity is required for LAPTM5-mediated CD3ζ degradation (data not shown), we next investigated whether these two proteins might interact in the lysosomal compartment. We stained spleen T cells before and after CD3 stimulation with anti-CD3ζ, anti-LAPTM5, and anti-LAMP1 to identify lysosomes. In unstimulated T cells, LAPTM5 was localized in lysosomes and CD3ζ was at the perimembrane region (Figure 6A, upper panels). However, after CD3 stimulation, a fraction of the CD3ζ translocated to the lysosomes, where it colocalized with LAPTM5 (Figure 6A, lower panels). To investigate whether LAPTM5 and CD3ζ interact, we prepared lysates from 2B4 cells expressing both LAPTM5 and CD3ζ by using a mild detergent, digitonin, and immunoprecipitated LAPTM5. Immunoblot analysis of the immunoprecipitates reproducibly detected the CD3ζ chain (Figure 6B and Figure S7). Curiously, much less CD3ζ was detected compared to the amount of LAPTM5. These results demonstrate that LAPTM5 and CD3ζ interact in the lysosomal compartment in T cells.

DISCUSSION

We have identified a lysosomal protein that negatively regulates surface TCR expression and T cell activation. LAPTM5 functions to downmodulate cell-surface TCR expression on DP thymocytes during T cell development and on peripheral T cells after CD3 stimulation. Deficiency in LAPTM5 results in elevated proliferation and cytokine production by T cells in response to CD3 stimulation in vitro, enhanced ex vivo responses, and prolonged DTH responses in vivo. Conversely, enforced expression of LAPTM5 results in reduced surface TCR amounts and reduced cytokine production. These results illustrate a unique

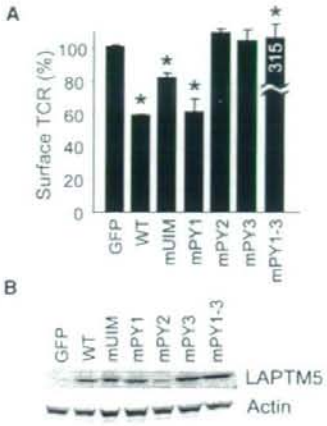

Figure 5. TCR Downmodulation Requires PY Motifs and the UIM of LAPTM5

(A) Ability of wild-type and mutant LAPTM5 to downmodulate surface TCR in 2B4 cells. Data are presented as percentage of TCRβ expression on GFP$^+$ versus GFP$^-$ cells. The results of three independent experiments (mean ± SD) are shown. *, $p < 0.001$ as compared with GFP-transduced cells (unpaired t test).

(B) Immunoblot analysis of wild-type and mutant LAPTM5 expression in sorted GFP$^+$ 2B4 cells transduced with each retrovirus.

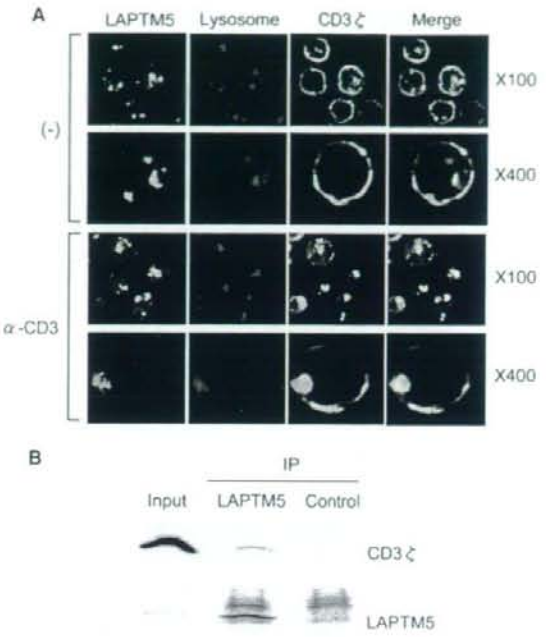

Figure 6. LAPTM5 and CD3ζ Colocalize in the Lysosome and Interact Physically

(A) Localization of LAPTM5, LAMP1, and CD3ζ in normal spleen T cells before (−) and after CD3 stimulation.

(B) Coprecipitation of LAPTM5 and CD3ζ. 2B4 cells expressing retrovirally transduced LAPTM5 and CD3ζ were lysed with digitonin and subjected to immunoprecipitation with antibodies against LAPTM5 or control rabbit IgG. The precipitates were resolved by SDS PAGE and blotted with antibodies against CD3ζ (upper panel) or LAPTM5 (lower panel).

mechanism for the regulation of surface TCR expression and T cell activation by a lysosomal protein.

Laptm5$^{-/-}$ and wild-type spleen T cells expressed similar amounts of cell-surface TCR in the resting state. After CD3 stimulation, *Laptm5*$^{-/-}$ T cells were able to downmodulate TCR, but the amounts of surface TCR were consistently higher than that found on wild-type T cells. Although the increase in the TCR expression on *Laptm5*$^{-/-}$ T cells was modest, one has to take into consideration the fact that the increased TCR expression was observed while the T cells were undergoing continuous downmodulation of surface TCR. Therefore, the cumulative physiological effect of the slightly increased TCR expression could be much greater and sufficient to cause T cell hyperactivation. It is worth noting that these assays were performed in the absence of pharmacologic agents such as protein-synthesis inhibitors. This straightforward assay allowed us to demonstrate an abnormality in TCR metabolism without any confounding artifacts, such as might be introduced by blocking new protein synthesis or excess manipulation of spleen T cells.

Several lines of evidence indicate that LAPTM5 regulates cell-surface TCR expression through the selective degradation of CD3ζ. First, anti-CD3-induced CD3ζ degradation was reduced in *Laptm5*$^{-/-}$ T cells, and this preceded and quantitatively correlated with the kinetics of the increased surface TCR. Second, LAPTM5 deficiency resulted in increased protein levels of CD3ζ in DP thymocytes as well as elevated surface expression of TCR. A similar phenotype has been observed in mice lacking SLAP or c-Cbl (Sosinowski et al., 2001; Naramura et al., 1998), although these mice had a greater increase in the expression of these molecules than the *Laptm5*$^{-/-}$ mice. The fact that SLAP and c-Cbl are both involved in the degradation of CD3ζ (Wang et al., 2001; Myers et al., 2005, 2006) is consistent with a role for LAPTM5 in mediating CD3ζ degradation. Third, enforced expression of LAPTM5 in 2B4 T cells resulted in decreased amounts of endogenous CD3ζ, reduced surface TCR expression, and diminished cytokine production, and transduction of exogenous CD3ζ restored surface TCR expression and T cell responses. Furthermore, enforced expression of LAPTM5 in normal spleen T cells also induced TCR downmodulation, which could be completely restored by coexpression of CD3ζ. This complementation experiment strongly supports a CD3ζ-chain-specific role for LAPTM5 in modulating cell-surface TCR expression. Fourth, LAPTM5 and CD3ζ interacted and colocalized in T cells. We conclude from these studies that LAPTM5 regulates cell-surface TCR expression and T cell activation by promoting CD3ζ degradation. However, the possibility that LAPTM5 may regulate T cell activation by targeting additional proteins cannot be excluded at this point. Because LAPTM5 deficiency resulted in only a partial inhibition of CD3ζ degradation, it is likely that both LAPTM5-dependent and -independent pathways mediate its degradation. The finding that overexpression of LAPTM5 alone caused a reduction of CD3ζ and a complete inhibition of TCR signaling in 2B4 cells further implies that the LAPTM5